UNIVERSITY OF PAVIA

FACULTY OF ENGINEERING

Department of Electrical, Computer and Biomedical Engineering

Master's Degree in Electrical Engineering

Transient Stability Assessment of Airport Electrical Power Systems under Large Disturbances and Electrification Scenarios: Analysis and Solutions for Milan Malpensa Airport

Valutazione della stabilità transitoria dei sistemi elettrici aeroportuali in presenza di grandi perturbazioni e scenari di elettrificazione: analisi e soluzioni per l'aeroporto di Milano Malpensa

Supervisor: Prof. Alessandro Bosisio

Industrial Supervisor: Eng.Martino Bosatra

Master Thesis of:

Yassine Zaibi

Academic Year 2024/2025

Acknowledgments

This thesis represents the culmination of my Master's studies and would not have been possible without the support, guidance, and contributions of several individuals and institutions.

First and foremost, I would like to express my deepest gratitude to my family for their constant support, patience, and encouragement throughout my academic journey. Their understanding and unwavering confidence in me have been fundamental during the demanding phases of my studies and the completion of this thesis.

I would like to extend my sincere gratitude to my supervisor Prof. Ing. Alessandro Bosisio for their continuous guidance, constructive feedback, and availability throughout the development of this work. Their technical insight and methodological rigor were fundamental in shaping both the analytical approach and the overall quality of this thesis.

I would also like to thank the academic staff of the Department for providing the theoretical foundations and practical knowledge that were essential for conducting this study. The courses and discussions throughout the program greatly contributed to my understanding of power systems, stability analysis, and protection engineering.

Special appreciation is extended to the professionals and institutions that provided technical documentation, system data, and operational insights related to the Milano Malpensa Airport electrical network. Their cooperation enabled a realistic and engineering oriented analysis of a complex critical infrastructure.

I am grateful to my colleagues and peers for their support, collaboration, and exchange of ideas during the course of my studies. Their feedback and discussions were instrumental in refining several aspects of this work.

Abstract

The reliable operation of an airport's electrical grid is fundamentally tied to the resilience and stability of its distribution network. This thesis investigates the transient behavior and fault tolerance of the Malpensa Airport power distribution system under a range of disturbance scenarios.

Using a simplified yet dynamically representative grid model, the study analyzes several fault conditions within the network, including a critical fault on the external Terna high voltage grid, faults occurring near or within A2A's generation facilities, and remote faults along the airport's low-voltage loops. These scenarios aim to assess the system's transient response, overall robustness, and flexibility in the presence of faults. As part of the airport's broader electrification and decarbonization initiatives, a 10 MW photovoltaic (PV) system will be integrated into the grid model. Consequently, the influence of this renewable energy source on the network's transient stability particularly during islanded operation must be thoroughly evaluated.

This thesis bridges the gap between renewable energy integration and grid stability by providing a framework to enhance the reliability of airport infrastructure through the assessment of transient resilience and fault tolerance.

Contents

List of Figures

List of Tables

Chapter 1

Introduction

1.1 Context and Motivation

Airports are among the most electricity dependent infrastructures in modern society. Virtually all operational domains including aircraft taxiing, air traffic control (ATC), runway lighting, terminal services, baggage handling, emergency systems, and security rely on an uninterrupted and stable supply of electrical power [1]. Even short duration disturbances on the order of a few hundred milliseconds can cause operational degradation, safety concerns, and significant economic losses [2]. As airports undergo increasing levels of digitization, automation, and electrification, their electrical networks have become correspondingly more complex and more critical to system reliability.

This trend is particularly evident in the integration of electrically powered ground support equipment, heat pumps, electric vehicle charging stations, and photovoltaic (PV) systems. Such developments alter energy flow patterns and load dynamics, introducing new challenges for maintaining electrical stability and resilience [1]. Ensuring that an airport's electrical infrastructure remains robust against both internal and external disturbances is therefore a fundamental requirement for maintaining safe and continuous operations [4].

Milan Malpensa Airport, the second largest airport in Italy and the principal aviation hub of the Lombardy region, is currently undergoing a substantial electrification phase. The planned incorporation of distributed energy resources, including a 10 MW photovoltaic installation, requires the maintenance of stringent reliability standards while accommodating increasingly dynamic load profiles. Quantifying the airport's capability to withstand and recover from electrical faults is thus strategically important for ensuring

long term operational resilience.

Modern airports also face significant challenges arising from perturbations external to the airport boundary. Disturbances originating from the national high voltage transmission grid operated by Terna may propagate into the airport's electrical network, generating voltage sags, frequency deviations, or even transient instability [5]. Additionally, faults occurring near A2A's generation facilities or within the airport's distribution system may impose further stress on equipment and compromise protection system performance .

Internally, the rapid growth of power electronics based loads and inverter dominated generation introduces dynamic behaviors markedly different from those of traditional synchronous machines. Photovoltaic plants, for example, contribute limited short-circuit current, tend to disconnect rapidly during severe voltage depressions, and exhibit control responses that must be carefully analyzed to assess their implications for transient and dynamic stability [3].

The combination of external grid disturbances, internal distribution faults, and evolving load and generation characteristics highlights the need for a comprehensive assessment of Malpensa Airport's electrical resilience. Insufficient understanding of these interactions may lead to miscoordination among protective devices, excessive tripping of critical loads, or cascading failures during contingency events [6]. For an airport of Malpensa's scale and strategic importance, such risks are unacceptable, making the study of its dynamic performance and vulnerabilities a fundamental operational priority.

1.2 Problem Statement

Milan Malpensa Airport relies on a complex electrical network composed of external HV connections, local generation, distribution loops, transformers, and a diverse portfolio of critical loads. This system must withstand a variety of disturbances without compromising safety or operations. However, several emerging factors raise concerns about the airport's resilience:

- External faults in the Terna HV grid may cause severe voltage dips or transients at Malpensa's point of connection.
- Disturbances near A2A's energy generation facilities can influence dynamic system responses.

- Faults within the internal medium voltage (MV) distribution loops can initiate fast transient events and challenge protection coordination.
- Increasing electrification of airport systems alters load dynamics, raises peak demand, and introduces a high share of power electronic devices.
- The integration of a large 10 MW PV plant affects transient stability, particularly during voltage sags.

The central problem addressed by this thesis is: How resilient and transiently stable is the Malpensa Airport electrical network when subjected to extreme external disturbances, internal faults, and future electrification scenarios by including the 10 MW PV integration?

Addressing this question requires transient stability simulation and a systematic evaluation of multiple disturbance categories.

1.3 Objectives of the Thesis

In this thesis, we present a comprehensive and model-based evaluation of the transient stability of the electrical network supplying Milan Malpensa Airport. To achieve this goal, the research is structured around the following objectives:

1. **Develop a representative ETAP model** of the airport's electrical network, accurately reflecting its operating characteristics, protection architecture, and dynamic components.
2. **Simulate and analyze the network's transient stability under severe disturbances**, including both external and internally induced contingency events.
3. **Model internal distribution faults within the airport** and evaluate their fault-clearing dynamics, protection performance, and voltage recovery behavior.
4. **Integrate a 10 MW photovoltaic plant into the network model** and assess its influence on the system's transient response and overall stability margins.
5. **Identify critical vulnerabilities and propose engineering solutions** aimed at improving system reliability, operational robustness, and resilience against electrical disturbances.

1.4 Methodology

This section outlines the methodological framework adopted to evaluate the transient stability and dynamic response of the electrical network supplying Milan Malpensa Airport. The process is organized into six main phases, moving from system characterization to model development, simulation, and resilience assessment.

Step 1: Data Acquisition and System Familiarization

The first phase focuses on understanding the structure, operating conditions, and external interfaces of the airport's electrical system. This includes:

- A detailed review of the topology of the Malpensa electrical network, including its medium-voltage loops, substations, and critical loads.
- An examination of the characteristics of the Terna high-voltage grid at the point of interconnection, with attention to fault levels, supply configuration, and relevant grid-code requirements.
- Analysis of the interface between the airport and the A2A generation plant, including the electrical behavior of the connection point.
- Collection and organization of technical data, such as load profiles, transformer and cable ratings, protection settings (where available), and the planned characteristics of the future 10 MW photovoltaic installation.

This phase ensures that the model accurately reflects the current and planned configuration of the airport network.

Step 2: Development of the Network Model in ETAP

Based on the collected data, a comprehensive ETAP model of the airport electrical system is constructed. The development process includes:

- Creating one-line diagrams representing the MV network architecture and the hierarchical structure of the system.
- Implementing all primary components, such as medium-voltage loops, transformers, buses, feeders, and major substations.
- Modeling loads using appropriate static or dynamic characteristics depending on their nature and sensitivity.

- Specifying protection devices, including relays, breakers, and fuses, and assigning their operational settings when available.

This step forms the digital representation of the system that will be used for subsequent simulations.

Step 3: Dynamic Component Modeling

To enable transient stability studies, the model is enhanced with dynamic representations of key components. This includes:

- Modeling turbo gas and steam turbine generators and backup power units with their associated controls, such as speed governors and excitation systems.
- Representing the photovoltaic plant as an inverter-based resource with standard control features suitable for transient analysis.
- Incorporating primary control loops, including automatic voltage regulators (AVR), governor systems, and inverter current-limiting functions.
- Selecting appropriate dynamic models from the ETAP library to ensure consistency with typical industry behavior.

This phase ensures that the model captures the time-dependent response of both conventional and inverter-based generation.

Step 4: Simulation of Disturbance Scenarios

A series of disturbance scenarios is defined to evaluate how the system behaves under severe and representative operating conditions. The simulated events include:

- High-voltage grid faults originating between Terna and A2A substation (e.g., three-phase faults and single-line-to-ground faults).
- Faults occurring at the nodes interfaced with the A2A generation plant.
- Internal distribution faults on medium-voltage lines feeding airport loads.
- Disturbances affecting the PV subsystem, including inverter disconnection scenarios.
- Electrification scenarios featuring increased power electronics based loads and higher energy demand.

These scenarios are selected to reflect realistic operating threats and future developments.

Step 5: Transient Stability and Protection Assessment

The system's dynamic performance is assessed by monitoring key stability indicators and protection behavior:

- Rotor-angle deviation of synchronous machines, where applicable.
- Voltage dips, overcurrents, and peak current conditions during faults.
- Critical Clearing Times (CCT) for selected disturbances and the time margins before loss of stability.
- Post-fault voltage recovery profiles and frequency response following major disturbances.

This analysis provides insights into the operational security of the system under adverse events.

Step 6: Resilience Evaluation and Mitigation Strategies

The final phase focuses on identifying vulnerabilities revealed during simulations and exploring potential measures to enhance system robustness. This includes:

- Highlighting weak points within the network, such as overloaded branches, insufficient protection coordination, or low-voltage recovery issues.
- Proposing operational improvements or structural reinforcements that could increase system reliability.
- Considering advanced technologies such as energy storage systems (ESS), STATCOM devices, and optimized relay coordination as potential solutions to strengthen the airport's resilience.

1.5 Limitations

This study is subject to several technical and practical limitations that constrain certain aspects of the analysis. To maintain reasonable simulation times while preserving consistent dynamic behavior, portions of the network have been simplified. On the low-voltage side, for example, loads are aggregated into lumped representations to capture overall behavior rather than device-level detail. With respect to the photovoltaic (PV) plant which is planned for future implementation planning parameters and inverter characteristics are represented using engineering estimates. These abstractions preserve the

qualitative dynamics of the system but may affect the numerical precision of specific results. A further limitation concerns data availability and recency. Certain information such as detailed protection relay configurations and time current characteristics was confidential or not fully accessible. In such cases, the study adopts well-justified engineering assumptions based on typical industry values and published practice. All assumptions are documented to support transparency and reproducibility. The thesis also excludes several topics that, while relevant to the broader context of power-system performance, fall outside the objectives of this work. These exclusions include detailed protection coordination and synchronization studies, long-term network planning and expansion analysis, and techno-economic assessments such as cost–benefit evaluations of upgrades or investment strategies. Likewise, power quality phenomena beyond voltage sags such as harmonic distortion and high-frequency disturbances are not considered, as they require a different modeling framework. Electromagnetic transient (EMT) phenomena at microsecond timescales are also out of scope; the analysis focuses on electromechanical and dynamic behavior over milliseconds to seconds. Finally, the absence of comprehensive historical disturbance records limits the extent of empirical validation. As a result, model validation relies on internal consistency checks across study types and on engineering judgment rather than direct event playback or one-to-one comparisons with measured oscillography. The results should therefore be interpreted as representative of system behavior under the examined conditions, not as exact replications of any specific past disturbance. Nevertheless, the modeling strives to reflect the real system as closely as possible by leveraging all available data such as transformer ratings, line and cable characteristics, generator parameters, and equipment ratings and types when constructing the network representation.

1.6 Structure of the Thesis

This thesis is organized as follows:

Chapter 1: introduces the context, motivation, problem, and objectives.

Chapter 2: presents the theoretical background for power system stability, PV dynamics, protection, and transient behavior.

Chapter 3: describes the modeling of the Malpensa Airport electrical system in ETAP.

Chapter 4: presents the Fault scenarios and assessment methodology

Chapter 5: presents the transient stability and fault simulation results under various scenarios, proposes solutions and strategies to enhance the airport's electrical resilience.

Chapter 6: concludes the work and outlines future research directions.

Chapter 2

Power System Dynamics and Transient Stability: Theoretical Background for System Analysis

2.1 Introduction

Transient stability and dynamic behavior are critical aspects of airport electrical networks. Airports rely on uninterrupted, high quality power to support air traffic control, navigation aids, radar installations, baggage handling, IT systems, and safety infrastructure.

Within the discipline of power system analysis, **stability** is defined as the ability of an electrical network to regain an acceptable operating equilibrium after a disturbance, while keeping voltages, currents, and machine angles within bounded limits. Stability therefore forms an essential part of the broader framework of *System Analysis Studies*, which includes load-flow analysis, short-circuit studies, contingency evaluation, and dynamic modeling [27, 28].

This chapter provides a comprehensive theoretical foundation supporting all dynamic simulations performed for the Malpensa Airport power system.

2.2 Power-Flow Studies

Power flow studies (also known as load-flow studies) are a fundamental analytical tool for evaluating the steady state behavior of power systems under balanced three phase operating conditions. Their principal objective is to determine the voltage magnitude and phase angle at every bus in the network [28]. Once bus voltages are known, real and reactive power flows through transmission lines, transformers, and all interconnected components can be computed, along with overall system losses [28].

2.2.1 Formulation of the Power-Flow Problem

Unlike basic circuit analysis, power flow calculations require solving a set of **nonlinear algebraic equations**. This nonlinearity arises because system loads are typically defined in terms of real and reactive power rather than impedance, and generators are modeled as controlled power injections instead of simple voltage or current sources [28]. At each bus k, the electrical state is represented by four variables:

- Voltage magnitude V_k
- Voltage phase angle δ_k
- Net real power injection P_k
- Net reactive power injection Q_k

For each bus, two of these quantities are specified as inputs, and the remaining two are solved for during the power-flow computation.

2.2.2 Bus Categorization

To solve the power flow equations efficiently, buses are categorized based on which variables are known. Instead of separate subsections, the three standard bus types are enumerated as follows:

1. **Swing (Slack) Bus** The swing bus serves as the global reference for voltage angle.
   - **Specified:** V, δ
   - **Computed:** P, Q

   It compensates for mismatch between total generation, load, and losses [27, 28].

2. **PQ (Load) Bus** Commonly used for load buses:

   - **Specified:** P, Q
   - **Computed:** V, δ

3. **PV (Voltage Controlled) Bus** Used when generators or voltage regulating equipment are present:

   - **Specified:** P, V
   - **Computed:** Q, δ

The interaction between the slack, PV, and PQ bus types, including the corresponding known and computed variables, is schematically illustrated in Figure 2.1.

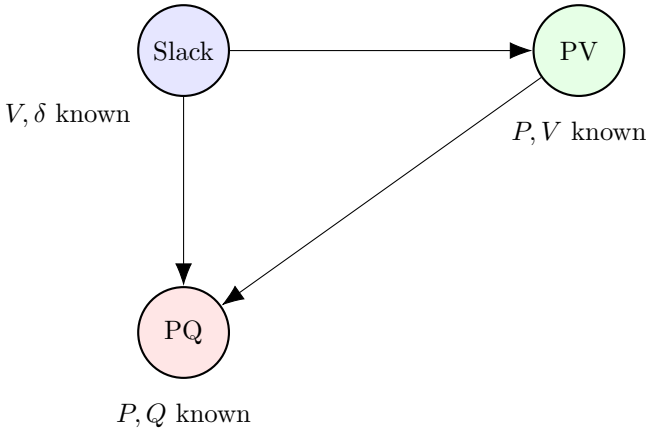

Figure 2.1: Illustration of the three standard bus types used in power-flow analysis.

2.2.3 Mathematical Formulation

The power flow problem is formulated using the bus admittance matrix $\mathbf{Y}_{\text{bus}}$, derived from transmission line impedances and transformer models. The nodal current-voltage relationship is:

$$\mathbf{I} = \mathbf{Y}_{\text{bus}}\mathbf{V}. \tag{2.1}$$

Since complex power at bus k is

$$S_k = P_k + jQ_k = V_k I_k^*, \tag{2.2}$$

substituting $I = Y_{\text{bus}}V$ yields the nonlinear power-flow equations:

$$P_k = V_k \sum_{m=1}^{n} V_m \left(G_{km}\cos(\delta_k - \delta_m) + B_{km}\sin(\delta_k - \delta_m)\right), \tag{2.3}$$

$$Q_k = V_k \sum_{m=1}^{n} V_m \left(G_{km}\sin(\delta_k - \delta_m) - B_{km}\cos(\delta_k - \delta_m)\right)., \tag{2.4}$$

The nodal current–voltage formulation described by (2.3)–(2.4) is schematically represented in Figure 2.2.

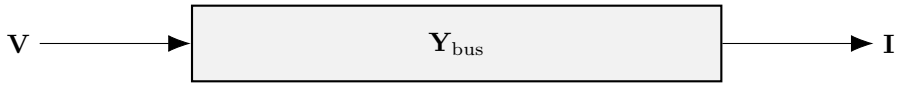

Figure 2.2: Nodal current-voltage relationship using $\mathbf{Y}_{\text{bus}}$.

2.2.4 Solution Methods

Because power-flow equations are nonlinear, iterative methods are required:

- **Gauss Seidel Method**: Simple but slow, rarely used in modern large systems.
- **Newton Raphson Method**: Industry standard; uses a Jacobian matrix and converges rapidly.
- **Fast-Decoupled Power Flow**: Approximation that exploits decoupling between P–δ and Q–V relationships; very fast for contingency studies.
- **DC Power Flow**: Linearized model neglecting Q and V magnitude variations; widely used for market and screening studies [27, 28].

2.2.5 Applications of Power-Flow Studies

Power-flow analysis supports essential grid engineering tasks, including:

- **System Planning** (evaluating new generators, loads, and transmission expansions)
- **Contingency Analysis** (N-1, N-2 outage screening)
- **Optimal Power Flow (OPF)** (minimizing losses or generation cost)
- **Steady-State Stability** (ensuring phase angle differences remain within safe limits) [27, 28]

2.3 Short Circuit Studies

Short circuit studies commonly referred to as fault studies represent a foundational component of power system analysis. Their primary purpose is to determine the magnitude and characteristics of currents that flow during abnormal or faulted operating conditions. Such analyses are essential for the correct specification of protective equipment, such as circuit breakers, fuses, and protective relays, ensuring that the power system can safely withstand and isolate electrical faults [28, 27].

2.3.1 Causes and Nature of Short Circuits

Short circuits are typically caused by insulation breakdown resulting from lightning-induced overvoltages, switching surges, contamination, aging, or mechanical failure [28, 27]. When faults occur, extremely large currents—often many times the rated operational current flow through the system. If not interrupted promptly, these currents may cause severe thermal heating of conductors and magnetic forces capable of damaging busbars and other equipment.

2.3.2 Types of Faults

- **Symmetrical (Three-Phase) Faults:** Involve all three phases shorted together. They occur infrequently (approximately 5% of cases), but produce the highest fault current magnitudes [28].
- **Unsymmetrical Faults:** Include:
  - Single line-to-ground (SLG) faults,
  - Line-to-line (LL) faults,
  - Double line-to-ground (DLG) faults.

  These faults require the method of symmetrical components, which decomposes the system into positive-, negative-, and zero-sequence networks [28].

2.3.3 Analytical Methodology

Short-circuit analysis relies on detailed component modeling.

- **Synchronous Machine Modeling**: Machines are represented by an internal voltage behind a series reactance that changes over time. For the initial high-magnitude

current, the sub-transient reactance (X''_d) is used; for intermediate periods, the transient reactance (X'_d) is used; and for steady-state fault levels, the synchronous reactance (X_d) is used [28, 27].

- **Bus Impedance Matrix $Z_{\mathbf{bus}}$**: Modern short-circuit programs compute fault currents using the bus impedance matrix

$$I_{\text{fault}} = \frac{V_{\text{prefault}}}{Z_{kk}} \tag{2.5}$$

where Z_{kk} is the Thévenin impedance at the faulted bus, while the off-diagonal elements determine the impact of a fault at one bus on the voltages of other buses [28].

Z_{11}	Z_{12}	Z_{13}
Z_{21}	Z_{22}	Z_{23}
Z_{31}	Z_{32}	Z_{33}

Figure 2.3: Conceptual bus impedance matrix for 3x3 Z_{bus}.

The Z_{bus} is more powerful than just finding fault current. For a fault at bus k, the voltage at any other bus i is:

$$V_i = V_{\text{prefault}} - \frac{Z_{ik}}{Z_{kk}} \cdot V_{\text{prefault}} \tag{2.6}$$

This uses the **off-diagonal** elements, showing why the full matrix matters. In general, three sequence networks are defined, each with its own bus impedance matrix: the positive sequence $Z^{(1)}_{\text{bus}}$, the negative sequence $Z^{(2)}_{\text{bus}}$, and the zero sequence $Z^{(0)}_{\text{bus}}$. The combination of sequence networks used in the fault analysis depends on the type of fault, as summarized in Table 2.1.

Fault Type	**Sequence Networks Involved**
Three-phase balanced	$Z^{(1)}_{\text{bus}}$ only
Single line-to-ground (SLG)	$Z^{(1)}_{\text{bus}}$, $Z^{(2)}_{\text{bus}}$, $Z^{(0)}_{\text{bus}}$
Line-to-line (LL)	$Z^{(1)}_{\text{bus}}$, $Z^{(2)}_{\text{bus}}$
Double line-to-ground (DLG)	$Z^{(1)}_{\text{bus}}$, $Z^{(2)}_{\text{bus}}$, $Z^{(0)}_{\text{bus}}$

Table 2.1: Sequence networks involved for each fault type.

For a balanced three-phase fault, only the positive sequence network is required,

and the fault current at bus k is given by:

$$I_{\text{fault}} = \frac{V_{\text{prefault}}}{Z_{kk}^{(1)}} \tag{2.7}$$

where $Z_{kk}^{(1)}$ is the Thévenin impedance of the positive sequence network at the faulted bus k. For unsymmetrical faults, the three sequence networks are interconnected according to the fault boundary conditions, following the method of symmetrical components. For instance, in the case of a single line-to-ground fault, the fault current is expressed as:

$$I_a^{(1)} = \frac{V_{\text{prefault}}}{Z_{kk}^{(1)} + Z_{kk}^{(2)} + Z_{kk}^{(0)}} \tag{2.8}$$

showing that all three sequence impedances contribute to limiting the fault current.

- **Fault Current Components**: The total short circuit current consists of an ac component (symmetrical) and a dc offset that decays exponentially according to the ratio X/R [27, 28].

$$i(t) = I_{\text{ac}}(t) + I_{\text{dc}}(t) \tag{2.9}$$

The time-domain behaviour of the asymmetrical short-circuit current, illustrating the superposition of the AC symmetrical component and the decaying DC offset, is shown in Figure 2.4.

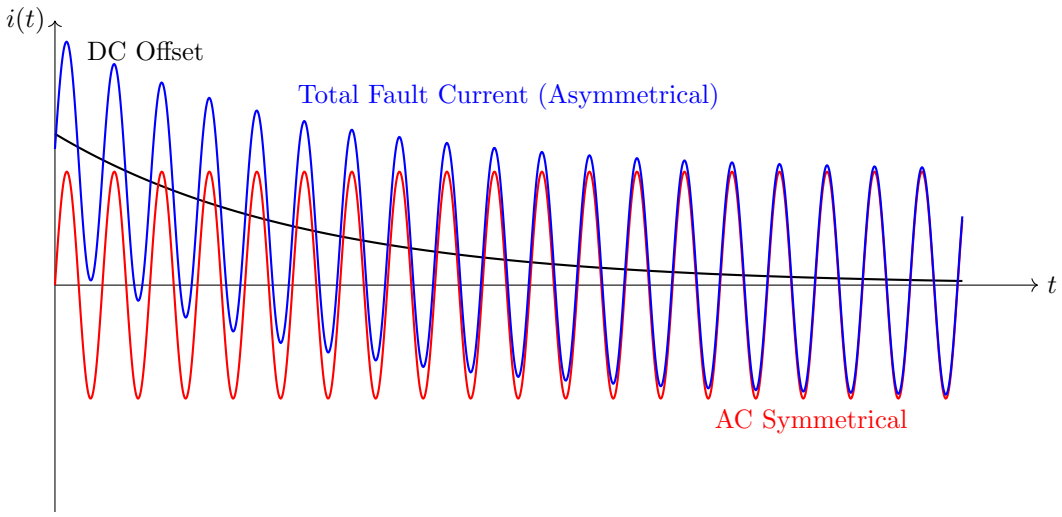

Figure 2.4: Asymmetrical short-circuit current components

2.3.4 Impact of Renewable Integration

The introduction of Distributed Generation (DG), particularly inverter-based and wind generation, significantly affects short-circuit behavior. Depending on the type, location, and penetration level of DG, fault current levels may either increase or decrease. Synchronous and induction based DG can increase fault levels, potentially exceeding the capacity of existing breakers. In contrast, inverter based DG typically contributes limited fault current, which may reduce overall fault levels, especially in weak or islanded systems. Additionally, DG can cause protection challenges such as blinding (where a relay fails to detect a fault) or nuisance tripping (where healthy sections are disconnected) due to the transition from unidirectional to bidirectional power flow [14, 19] and this is illustrated in Figure 2.5.

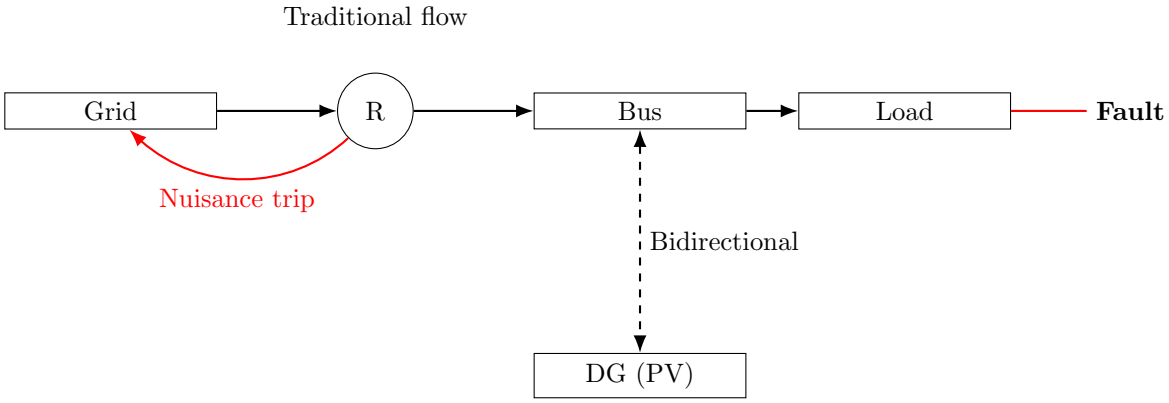

Figure 2.5: Illustration of nuisance tripping due to bidirectional power flow introduced by distributed generation.

2.3.5 Selection of Protective Equipment

Short-circuit studies directly inform the specification and coordination of protective devices:

Circuit Breakers Breakers must be rated for:

- **Symmetrical interrupting current**, which must exceed the calculated symmetrical fault current
- **Momentary current**, which accounts for the asymmetrical (peak) current, typically approximated by multiplying the subtransient current by an asymmetry factor (commonly around 1.6) [28].

Fuses: Fuses are single-operation clearing devices selected using time–current characteristic (TCC) curves to ensure they operate faster than upstream protection and

maintain coordination [28].

Relay Coordination: Short-circuit results allow engineers to establish selective coordination, ensuring that only the device nearest the fault operates while upstream devices remain closed. This principle minimizes the extent of outages and improves overall system reliability.

2.4 Power System Security: Contingency and Transient Overvoltage Studies

Within the broader framework of power system analysis, contingency analysis and transient overvoltage studies represent two critical pillars for ensuring system security, reliability, and equipment protection. While contingency analysis addresses the steady-state consequences of equipment outages, transient overvoltage studies examine high-frequency electromagnetic disturbances that can compromise insulation integrity and operational continuity. Together, these complementary disciplines form the foundation of modern power system planning and operation [28].

2.4.1 Contingency Analysis

Contingency analysis is a computer aided procedure used to evaluate the impact of planned or unplanned outages of system components such as transmission lines, transformers, generators, or major loads [28]. Its purpose is to assess whether the network can continue to operate within acceptable voltage, thermal, and stability limits once an element has been removed from service. Contingency assessment is an integral part of real time and planning stage security analysis in modern power system operation.

To determine the post outage operating point, various computational methods are employed:

- **Full AC Power Flow Solutions:** High–precision methods (e.g., Newton Raphson or Fast–Decoupled power flow) compute the new steady state voltages and line flows after an outage [27].
- **Linear Distribution Factors:** Line Outage Distribution Factors (LODFs) and Power Transfer Distribution Factors (PTDFs), often derived from the bus impedance

matrix Z_{bus}, allow rapid estimation of line overloads across hundreds of possible contingencies [27].

- **DC Power Flow:** A simplified linear model suitable for screening large numbers of contingencies where only real power flows are of interest [28].

The concept of a transmission line outage as a contingency event is schematically illustrated in Figure 2.6.

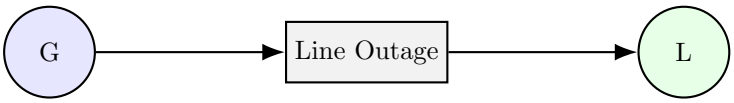

Figure 2.6: Conceptual diagram of a line outage used in contingency analysis.

2.4.1.1 Security Assessment and Operating Criteria

A central objective of contingency analysis is to ensure that the system satisfies predefined security standards following the loss of any major component. The most widely adopted rule is the **N-1 criterion**, which states that the system must remain within acceptable ratings even after the outage of a single generation or transmission element. More demanding requirements, such as N-2 or probabilistic criteria, may be applied for critical infrastructures where uninterrupted operation is mandatory [14].

Although originally developed for transmission networks, the N-1 criterion is increasingly applied within medium voltage distribution systems, particularly in facilities where supply continuity is mission critical. Airports fall firmly into this category: even a single feeder or transformer outage may directly impact air traffic control, navigation systems, terminal operations, or safety critical infrastructure. For this reason, the airport's internal distribution system, including on-site generation, must be evaluated against N-1 contingencies to ensure that essential services are not compromised.

Security assessment evaluates:

- Post contingency bus voltage magnitudes,
- Thermal loading of transmission lines and transformers,
- Potential cascading effects due to overloads,
- Risk of voltage instability or loss of synchronism.

This process supports both day–ahead planning and real time operation, ensuring that no single failure compromises the overall system integrity.

The impact of a contingency on line thermal loading, including the transition from pre-contingency to post-contingency operating conditions, is schematically illustrated in Figure 2.7.

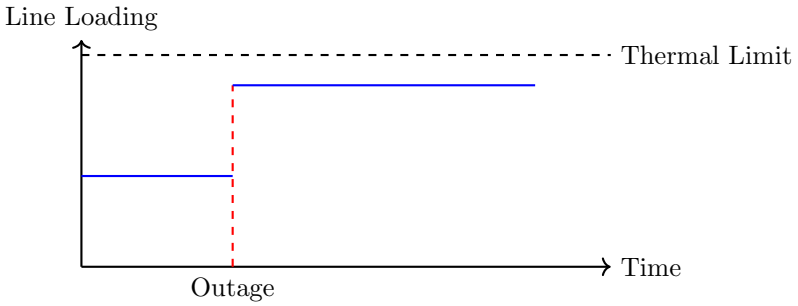

Figure 2.7: line loading transitioning from pre–contingency to post contingency state.

2.4.1.2 Operational Importance

Contingency analysis plays an indispensable role in operational planning, congestion management, and preventive control. System operators rely on real time contingency analysis (RTCA) tools to determine whether the grid can withstand sudden equipment outages and to identify corrective actions such as generation redispatch, topology changes, or controlled load shedding.

Historical events such as the 2003 Northeast blackout demonstrated that inadequate contingency evaluation, combined with poor situational awareness, can escalate minor events into widespread system collapses [28]. As a result, modern energy management systems continuously screen N-1 and higher order contingencies to maintain system security.

2.4.2 Transient Overvoltage Studies

Transient overvoltage studies investigate the magnitude, duration, and propagation of surges that arise from both external and internal disturbances. These transient events propagate as traveling waves along transmission lines, often approaching the speed of light, and can impose severe electrical stress on insulation systems. The relationship between a transient lightning overvoltage and the Basic Insulation Level (BIL) is shown in Figure 2.8.

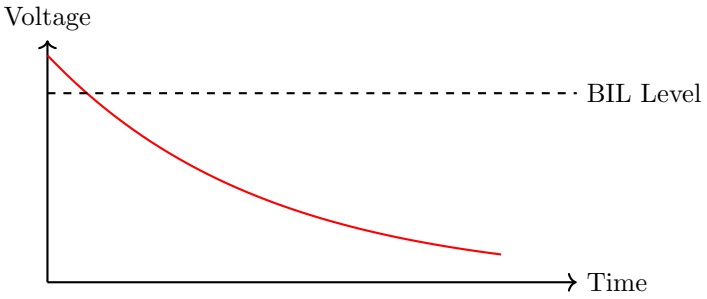

Figure 2.8: Typical lightning surge waveform relative to basic insulation withstand level (BIL).

2.4.2.1 Sources and Characteristics of Overvoltages

Two principal categories of transient overvoltages are considered:

- **Lightning Surges:** Produced by direct or induced lightning strokes, characterized by extremely rapid rise times (on the order of microseconds) and high peak voltages. They are the dominant overvoltage concern for overhead transmission systems below approximately 230 kV.
- **Switching Surges:** Generated by internal switching operations such as energizing long transmission lines, transformer energization, or breaker reclosing. Switching surges typically dominate insulation design at EHV levels above 345 kV.

To mitigate overvoltages:

- **Insulation coordination** ensures equipment withstand ratings exceed predicted surge magnitudes.
- **Surge arresters**, typically metal-oxide varistors (MOVs), limit transient peaks and protect equipment.
- **Pre-insertion resistors** or controlled switching schemes in EHV breakers reduce switching surge magnitude.

2.5 Stability Analysis

2.5.1 Synchronous Generator Dynamics

Understanding the dynamic behaviour of synchronous generators is fundamental to any transient stability study. A synchronous machine converts mechanical power into electrical power through electromagnetic coupling between a rotating magnetic field on the

rotor and a set of three-phase armature windings on the stator. Each synchronous machine is represented by a simplified equivalent circuit consisting of an internal transient voltage E'_i in series with the transient reactance X'_d, as shown in Fig 2.9.

This representation differs from the steady-state model, where the synchronous reactance X_d is used together with the internal voltage E_i. The use of X'_d reflects the short-term electromagnetic dynamics of the rotor circuits immediately following a disturbance, before steady-state conditions are re-established [27].

Neglecting armature resistance, which is typically small compared to the reactance, the terminal voltage V_t can be expressed as:

$$V_t = E'_i - jX'_d I \tag{2.10}$$

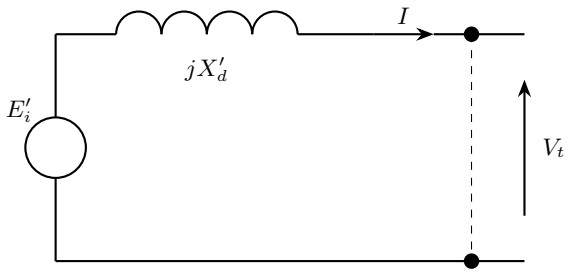

(a)

Figure 2.9: Equivalent circuit of a synchronous machine for transient stability studies

The associated phasor diagram shown in Figure 2.10 illustrates the relationship between E'_i, V_t, and the voltage drop across the transient reactance jX'_d. The internal voltage E'_i leads the terminal voltage V_t by the rotor angle δ, which is the key variable governing power transfer and rotor dynamics. All phasor quantities are defined with respect to a common system reference frame, allowing consistent analysis of interconnected machines within the network [13].

In steady-state operation, the rotor spins at constant synchronous speed, and the electrical torque developed in the machine balances the mechanical torque supplied by the prime mover. Any deviation from this equilibrium results in a mismatch between mechanical and electrical power, causing the rotor speed and its electrical phase angle to change [13].

The dynamic behaviour of the generator rotor is described by the *swing equation*, a second-order nonlinear differential equation obtained from Newton's law of rotational motion. According to [29] and IEEE modeling guides [26], the swing equation in per-unit

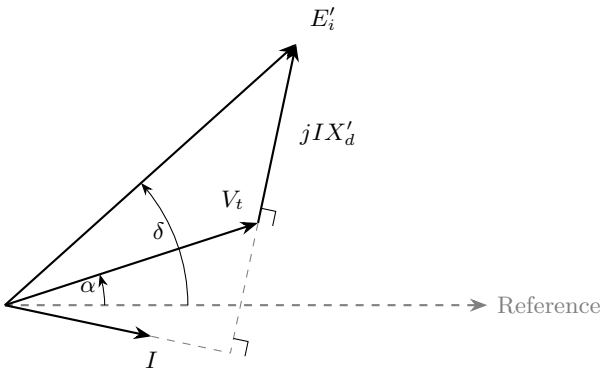

Figure 2.10: Phasor diagram: $E_i' = V_t + jIX_d'$

form is expressed as

$$M\frac{d^2\delta}{dt^2} = P_m - P_e, \tag{2.11}$$

where δ is the rotor electrical angle measured with respect to a synchronously rotating reference frame, P_m is the mechanical input power, P_e is the electrical output power, and M relates the generator's stored kinetic energy to its rated apparent power. For a synchronous generator operating at synchronous speed ω_s, the inertia constant is defined as

$$M = \frac{2H}{\omega_s}, \tag{2.12}$$

where H (in seconds) is the per-unit inertia constant representing the stored kinetic energy in megajoules per MVA of rated capacity [27].

A larger inertia constant implies that rotor speed and therefore electrical frequency changes more slowly following a disturbance. Generators found in airport environments typically have relatively low inertia values compared to large utility scale generators, making them more sensitive to abrupt power imbalances. When a disturbance such as a short circuit occurs, P_e drops substantially due to increased network impedance and voltage depression. Because P_m remains nearly constant, the rotor experiences accelerating torque, causing δ to increase. After the fault is cleared, P_e rises again, providing decelerating power. Stability is maintained only if the decelerating energy is sufficient to counteract the accumulated accelerating energy [13].

Synchronous generator models used in transient stability studies rely heavily on $dq0$ reference frame representations, in which the stator equations are expressed in rotating coordinates aligned with the rotor magnetic field. This representation simplifies the coupling between flux, current, and torque, and forms the foundation of all standard

generator models used in commercial simulation tools such as ETAP, PSS E, and PowerFactory [25].

2.5.2 Reference Frame Transformations

The mathematical analysis of three-phase machines and power electronic converters is facilitated by transforming variables from the natural *abc* frame into orthogonal coordinate systems. Reference frame transformations reduce the complexity of sinusoidal three-phase quantities by representing them either as stationary orthogonal components ($\alpha\beta 0$) or as constant quantities in a synchronously rotating frame ($dq0$).

2.5.2.1 Clarke Transformation

The Clarke transformation projects the three-phase *abc* variables onto a stationary $\alpha\beta 0$ frame according to

$$\begin{bmatrix} i_\alpha \\ i_\beta \\ i_0 \end{bmatrix} = \frac{2}{3} \begin{bmatrix} 1 & -\frac{1}{2} & -\frac{1}{2} \\ 0 & \frac{\sqrt{3}}{2} & -\frac{\sqrt{3}}{2} \\ \frac{1}{2} & \frac{1}{2} & \frac{1}{2} \end{bmatrix} \begin{bmatrix} i_a \\ i_b \\ i_c \end{bmatrix}. \tag{2.13}$$

For balanced systems, the zero-sequence component i_0 vanishes. The α and β components represent a single rotating space vector that captures the instantaneous magnitude and phase of the three-phase system [29].

2.5.2.2 Park Transformation

The Park transformation rotates the stationary $\alpha\beta 0$ frame into a synchronously rotating $dq0$ frame using the transformation

$$\begin{bmatrix} i_d \\ i_q \\ i_0 \end{bmatrix} = \begin{bmatrix} \cos\theta & \sin\theta & 0 \\ -\sin\theta & \cos\theta & 0 \\ 0 & 0 & 1 \end{bmatrix} \begin{bmatrix} i_\alpha \\ i_\beta \\ i_0 \end{bmatrix}, \tag{2.14}$$

where θ tracks the electrical rotor position. When the rotating frame is aligned with the rotor magnetic field, the electrical quantities in the dq axes become *constant* under balanced steady-state operation. This greatly simplifies the modeling of machine flux linkages, electromagnetic torque, and control loops.

The dq representation is particularly important for rotor angle stability, because the rotor electrical angle δ is precisely the angular displacement between the generator's d-

axis and the infinite bus voltage reference. Hence, deviations in δ are directly represented in the dq model, making it the natural coordinate system for transient stability studies [28, 27].

2.5.3 Rotor Angle Stability

Rotor angle stability concerns the ability of synchronous machines to remain in synchronism after disturbances. It is governed by the interaction of mechanical input power, electrical output power, and the restoring (synchronizing) torque provided by the network.

In classical analysis, the electrical power transfer of a generator connected through reactance X to a strong grid is given by the power-angle relationship

$$P_e = \frac{EV}{X} \sin \delta, \tag{2.15}$$

where E is the internal electromotive force of the machine, and V is the terminal or infinite bus voltage. The slope of this curve determines the synchronizing torque coefficient:

$$P_{\text{syn}} = \frac{dP_e}{d\delta} = \frac{EV}{X} \cos \delta. \tag{2.16}$$

When δ approaches $90°$, $\cos \delta$ approaches zero, and the system loses synchronizing torque, making it highly vulnerable to instability. During faults, voltage drops reduce E and V, and the effective reactance increases, further weakening synchronizing torque. In Malpensa airport power systems characterized by turbo gas and steam turbine generators with relatively low inertia this reduction in synchronizing torque can rapidly lead to loss of synchronism if clearing times are not sufficiently fast.

2.5.4 Single Machine Infinite Bus (SMIB) Model

The SMIB model provides a simplified yet powerful representation of the dynamics of a single generator connected to a large power system with very high inertia. An infinite bus has constant voltage, constant frequency, and infinite short circuit strength. Because transmission operators such as Terna maintain very high system stiffness, an airport generator connected to such a grid behaves nearly identically to a SMIB system, this is represented in Figure 2.11.

The SMIB model is widely used to develop analytical tools for stability assessment,

including the synchronizing torque coefficient and the Equal-Area Criterion. It allows direct interpretation of the influence of network reactance, fault location, and clearing time on generator stability. Although it represents the simplest case of transient stability, it forms the basis for understanding more complex multimachine interactions. Terna behaves as an infinite bus: constant voltage, constant frequency, and extremely high short-circuit strength.

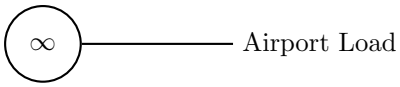

Figure 2.11: Infinite bus representation of Terna relative to Malpensa Airport.

2.5.5 Equal-Area Criterion

The Equal-Area Criterion (EAC) Figure 2.12 provides a graphical method for assessing the transient stability of a SMIB system. During a fault, the electrical power output drops, producing an accelerating area on the power-angle curve. When the fault is cleared, the electrical power exceeds the mechanical input, producing a decelerating area. The system remains stable if and only if the decelerating area is equal to or greater than the accelerating area. This criterion provides direct insight into *critical clearing time*, the maximum allowable duration of a fault before loss of synchronism becomes inevitable.

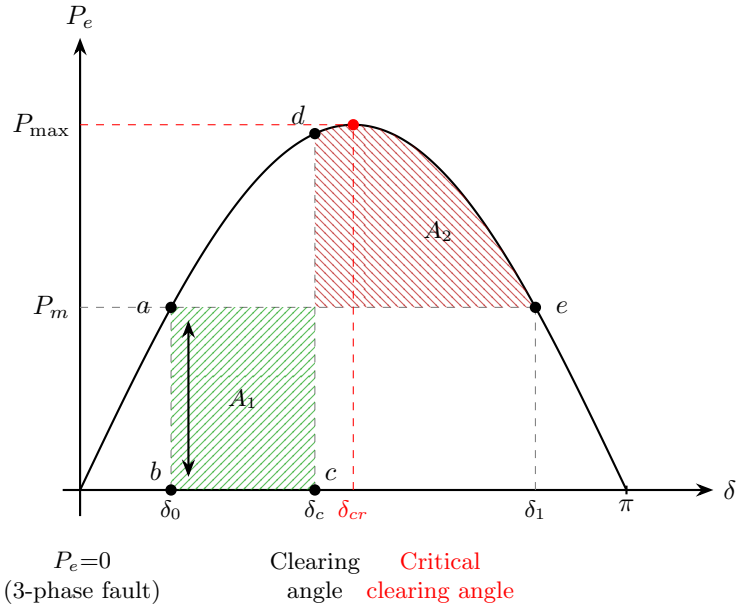

Figure 2.12: Equal area criterion for a three-phase fault ($P_e = 0$): green area A_1 is the accelerating energy and red area A_2 is the decelerating energy.

While the Equal Area Criterion provides valuable insight for simple SMIB systems,

real power networks require more advanced tools for stability evaluation. For multimachine systems, time domain simulations numerically solve the swing equations for all generators, capturing detailed rotor angle trajectories over time [27]. These simulations account for network topology, protection actions, AVR and governor dynamics, and the interaction between synchronous and inverter based sources.

For assessing small signal stability, eigenvalue analysis is used to linearize the system around an operating point and compute the damping and frequency of oscillatory modes. Negative real parts of eigenvalues indicate stable modes with decaying oscillations, while poorly damped inter-area modes may require power-system stabilizers (PSS) or revised operating conditions.

2.5.6 Coherency in Multimachine Systems

In interconnected networks containing multiple synchronous generators, certain machines tend to "swing together" during disturbances. These machines, which exhibit nearly identical rotor angle trajectories, are said to be coherent [27]. Coherency is a key concept in reducing multimachine models into equivalent representations, enabling simpler stability assessment. Coherent groups form the basis of controlled islanding, inter-area mode analysis, and the design of power system stabilizers.

Although an airport network typically includes only a small number of synchronous machines, the concept of coherency remains relevant when multiple generators operate in parallel or during transitions between grid connected and islanded modes. In such configurations, even with differing inertia constants, machines that are electrically coupled tend to exhibit approximately coherent behavior. Maintaining this approximate coherency during disturbances is essential for preventing loss of synchronism and ensuring reliable supply to airport critical loads.

The distinction between coherent and non-coherent generator behaviour, expressed in terms of rotor-angle trajectories during disturbances, is shown in Figure 2.13.

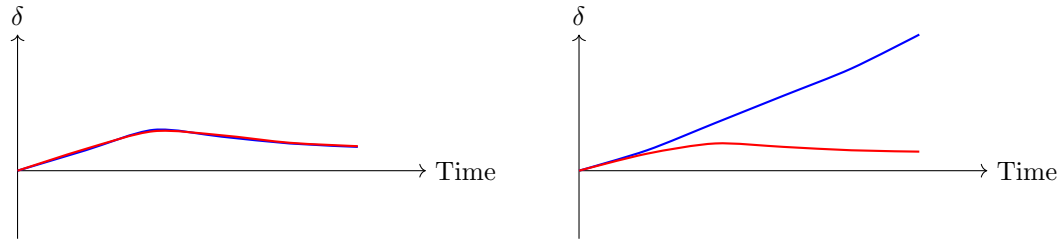

(a) Coherent generators (similar trajectories).

(b) Non-coherent generators (diverging trajectories).

Figure 2.13: Coherency vs non-coherency in multimachine systems.

2.6 Frequency and Voltage Stability

Frequency stability and voltage stability constitute two of the fundamental categories of power system stability. Although they describe different physical mechanisms, they are closely interconnected in practical electrical networks. Frequency stability concerns the system's ability to maintain the nominal frequency following real power imbalances, whereas voltage stability is governed by the system's ability to supply adequate reactive power to maintain acceptable voltage magnitudes [24].

2.6.1 Frequency Stability

Frequency stability is defined as the ability of a power system to maintain or restore its nominal frequency following disturbances that cause significant imbalances between total generation and load [22]. In synchronous power systems, frequency is directly proportional to the rotational speed of synchronous generators. When a disturbance occurs, such as the sudden loss of a generating unit, the mismatch between mechanical input power and electrical output power causes the generator rotors to accelerate or decelerate.

This dynamic is governed by the swing equation:

$$2H\omega_s \frac{d\omega}{dt} = P_m - P_e, \tag{2.17}$$

where H is the inertia constant, ω_s the synchronous angular speed, P_m the mechanical input power, and P_e the electrical output power [24]. The inertia constant determines the Rate-of-Change-of-Frequency (RoCoF). A low inertia system will exhibit faster and deeper frequency excursions compared to a high inertia system.

Frequency stability is supported by multiple layers of control:

- **Inertial response**: an immediate, sub-second contribution of real power from the stored kinetic energy of synchronous machines.
- **Primary frequency control**: autonomous governor action that adjusts mechanical input power based on frequency deviation.
- **Secondary control (AGC)**: slower centralized control that restores frequency to its nominal value.

A typical system frequency response following a generation loss is shown in Figure 2.14.

In systems with high PV or wind penetration, frequency stability becomes more challenging because inverter based resources do not inherently provide inertia or governor response. Without synthetic inertia or fast frequency response control, frequency nadirs become deeper, and RoCoF increases [23].

Under Frequency Load Shedding (UFLS) is used as an emergency action during severe disturbances. UFLS primarily limits the *minimum* frequency reached (the frequency nadir), rather than restoring frequency. Complete frequency recovery requires governor and AGC mechanisms.

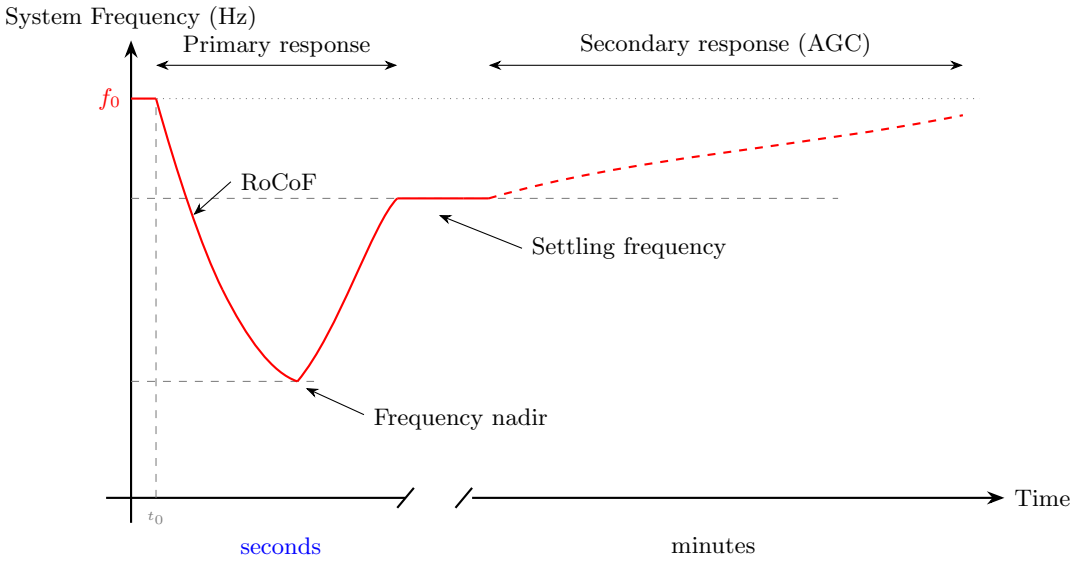

Figure 2.14: System frequency response following a generation loss event: RoCoF, frequency nadir, primary response, and secondary response (AGC).

2.6.2 Voltage Stability, relationship Between Voltage and Reactive Power

Voltage stability refers to the ability of a power system to maintain acceptable voltage magnitudes at all buses following a disturbance. It is dominated by reactive power balance. Voltage instability occurs when the system cannot supply the reactive power required by loads, resulting in progressive voltage decline [27].

In AC power systems, voltage magnitude is governed primarily by the local balance of reactive power rather than active power. This fundamental relationship arises from the power flow equations, where the voltage drop across a line of impedance $Z = R + jX$ is approximated as [28]:

$$\Delta V \approx \frac{PR + QX}{V} \tag{2.18}$$

The relative influence of active and reactive power on voltage depends strongly on the network level under consideration, as the resistance-to- reactance ratio (R/X) differs significantly between transmission and distribution systems [28].

2.6.2.1 Transmission Systems

At high voltage transmission levels, line reactance dominates such that $X \gg R$, and equation (2.18) simplifies to:

$$\Delta V \approx \frac{QX}{V} \tag{2.19}$$

In this regime, voltage is predominantly controlled by reactive power flow, while active power primarily governs the rotor angle and system frequency. Reactive power cannot be transported efficiently over long distances and must therefore be supplied locally through generator excitation, capacitor banks, or flexible AC transmission system (FACTS) devices [27].

2.6.2.2 Distribution Systems

At medium and low voltage distribution levels, line resistance becomes comparable to or greater than reactance ($R \approx X$ or $R > X$), particularly in low voltage cables [27, 29]. In this case, neither term in equation (2.18) can be neglected, and both active and reactive power contribute meaningfully to voltage variations. This has two important

consequences:

- Active power curtailment or redistribution becomes an effective tool for voltage regulation, in addition to reactive power control [27, 29, 28].
- Reactive power compensation alone is less effective than at transmission level, and must be combined with active power management for adequate voltage control [27, 29, 28].

In the context of airport distribution networks, this is particularly relevant as the system operates primarily at medium voltage (typically 6.6 kV to 33 kV) with underground cables characterized by high R/X ratios. The combined effect of motor starting transients, large HVAC loads, and ground support equipment imposes simultaneous active and reactive power demands that must both be considered in voltage stability assessment [28].

2.6.2.3 Voltage Collapse Mechanism

Regardless of the network level, when reactive demand exceeds local supply capacity the system enters a regime of progressive voltage decline. As load increases and reactive demand grows, generators approach their reactive capability limits and their Over-Excitation Limiters (OEL) activate, restricting further reactive output. The resulting voltage drop causes motor loads to draw increased current to maintain constant power, consuming additional reactive power in line impedances and further depressing voltage. This positive feedback mechanism can lead to voltage collapse if not mitigated by corrective action [27].

This behavior is captured graphically by the PV nose curve shown in Figure 2.15, where the critical point at $P_{\max}$ represents the boundary beyond which voltage equilibrium can no longer be maintained. In islanded airport operation, the reactive power reserve of the generators represents a hard constraint on the maximum supportable load, making reactive power planning a critical design criterion [27].

Voltage stability is often assessed through:

- **PV (P–V) curves**, which show the relationship between voltage magnitude and load power.
- **Q–V curves**, which depict the amount of reactive power needed to maintain voltage at a particular bus.

At the "nose point" of the PV curve, the system reaches maximum loadability. Beyond this point, no stable operating voltage exists Figure 2.15.

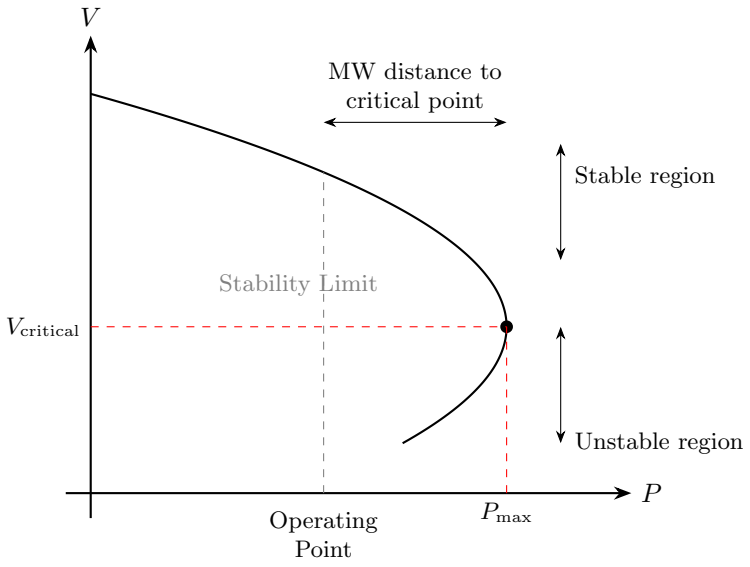

Figure 2.15: PV nose curve illustrating the voltage stability limit

Reactive power compensation devices such as capacitor banks, SVCs, and STATCOMs improve voltage stability by supplying reactive power during disturbances. However, static capacitors provide reactive power proportional to V^2, making them less effective during low-voltage conditions. STATCOMs, by contrast, can maintain reactive current output even at depressed voltage levels, making them highly effective against voltage collapse [27, 28].

Load type also influences voltage stability. Constant impedance loads reduce their reactive consumption as voltage drops, aiding stability. Constant current loads reduce power proportionally with voltage. However, constant power loads including many electronic and motor loads draw *increasing* current as voltage decreases, sharply raising reactive power demand and worsening instability.

2.6.3 Interaction Between Frequency and Voltage Stability

Although frequency and voltage stability are classified separately, they are tightly coupled. A large voltage depression reduces generator electrical power output according to

$$P_e = \frac{EV}{X} \sin \delta, \tag{2.20}$$

which increases accelerating torque and contributes to frequency decline. Conversely, frequency related events influence voltage by altering power flows, reactive power requirements, and generator excitation limits [27].

Modern grid forming inverters and VSC-HVDC converters enhance both frequency and voltage stability by independently regulating active and reactive power with fast dynamic response. Their ability to emulate inertia and provide voltage support makes them increasingly valuable in systems with high penetrations of renewable energy sources.

2.7 Chapter Summary

This chapter established the theoretical foundation for modeling and analyzing power system transient stability. The concepts presented here inform all subsequent simulations and engineering decisions throughout the thesis.

Chapter 3

System Modelling for Transient Stability Analysis

3.1 Introduction

Accurate transient stability analysis requires a modelling framework capable of representing the key electromechanical dynamics of synchronous generators, the behaviour of inverter-based photovoltaic (PV) resources, the characteristics of the electrical network, and the influence of protection systems on fault clearing and system recovery. In this study, the Malpensa Airport electrical power system is modelled using the Transient Stability module of ETAP. The modelling approach follows the established methodologies documented in classical stability literature such as Kundur [29] and IEEE guideline IEEE Std. 1110–2002/2019 [26].

The philosophy adopted balances computational efficiency with adequate dynamic fidelity. Detailed models are applied to components whose behaviour strongly influences transient stability namely synchronous generators, excitation and governor systems, inverter based generation, and the external grid whereas aggregated and equivalent representations are applied to subsystems whose internal details have limited influence on electromechanical behaviour (e.g., LV distribution feeders and individual loads). This ensures that rotor-angle swings, voltage recovery, frequency deviations, and protection interactions are all faithfully represented without unnecessary model complexity.

This chapter presents the full modelling framework, including load modelling and network equivalencing, synchronous generator representation, transmission network ab-

straction, PV system modelling, detailed fault representation, protection modelling, coordination interpretation, generator tripping logic, and inverter behaviour during disturbances. These elements form the technical basis for the transient stability simulations and analyses presented in later chapters.

3.2 Milano Malpensa Airport Network

The electrical and energy infrastructure of Milano Malpensa Airport constitutes a highly integrated and mission critical system whose primary objective is to guarantee uninterrupted, safe, and reliable supply of electricity, thermal energy, and chilled water to all airport operations. At the heart of this infrastructure lies the **Centrale di Malpensa**, a thermoelectric trigeneration plant that operates within a **Closed Distribution System (SDC)** managed by SEA. The plant and associated grid architecture are formally classified as "relevant and strategic," given their fundamental role in ensuring the operational continuity and security of the entire airport.

3.2.1 Centrale di Malpensa: Location and Infrastructure

The trigeneration plant is situated in the south–west sector of the airport (sedime) and occupies an area of approximately 13,870 m^2. The facility comprises several functional zones:

- **Main Plant Area**: Hosts the trigeneration machinery, internal access roads, auxiliary piping, and landscaped green areas.
- **Administrative Building ("Palazzina Uffici")**: A three storey structure housing the control room, supervision and automation systems, auxiliary services, and administrative offices.
- **Auxiliary Technical Structures**: Including turbine enclosures, gas compressor sheds, mechanical workshops, storage warehouses, and electrical rooms.

This integrated layout ensures the complete autonomy of operational processes, allowing 24/7 production of all energy vectors required by airport systems.

3.2.2 Functional Role of the Trigeneration Plant

The Centrale di Malpensa is designed to produce simultaneously three essential forms of energy:

- **Electric Energy**: Distributed through the internal MV network to terminals, runways, baggage facilities, cargo areas, and support buildings.
- **Thermal Energy**: Delivered primarily as hot water for the heating of passenger terminals and administrative buildings.
- **Cooling Energy**: Generated as chilled water to satisfy the substantial air conditioning and industrial cooling requirements of airport infrastructures.

The trigeneration configuration results in higher efficiency, fuel savings, and improved environmental performance, while ensuring the energy resilience required by a major international hub.

3.2.3 Technical Composition of the Generation Units

The plant is organised into two **combined cycles**, each consisting of a gas turbine and an associated steam turbine driven by recovered exhaust heat:

- **Combined Cycle 1**:
  - Gas Turbine G3: 25 MW
  - Steam Turbine G4: 5 MW
- **Combined Cycle 2**:
  - Gas Turbine G6: 30 MW
  - Steam Turbine G5: 8 MW

This configuration provides operational flexibility, redundancy, and high availability, ensuring continuous service even during maintenance or partial outages.

3.2.4 Integration into the Closed Distribution System (SDC)

The Milano Malpensa electrical grid is formally recognised as a **Closed Distribution System** and is managed by SEA in its role as distributor. This internal grid includes all transformation, switching, distribution, and protection systems and is electrically and administratively distinct from the public networks.

The SDC is structured on two primary voltage levels:

High Voltage (AT – 132 kV)

This subsystem provides the interface with the national transmission network. Key components include:

- Direct connection to the **Rete di Trasmissione Nazionale (RTN)** operated by Terna.
- Three main step up transformers (**TRS1, TRS2, TRS3**) that couple the combined cycles to the 132 kV system.
- High voltage switching and protection apparatus for selective isolation and reconfiguration.

Medium Voltage (MT – 15 kV)

The MV level distributes power to all airport loads, including:

- Passengers terminals and HVAC systems
- Airfield lighting and navigational aids
- Baggage handling systems
- Cargo and logistics facilities
- Auxiliary buildings and landside infrastructure

The MV network is engineered to ensure high reliability, fast protection coordination, and the capability to maintain service continuity under fault conditions.

3.2.5 Connections, Redundancy, and Islanding Capability

Maintaining the continuity of electrical supply is indispensable for airport safety and operations. For this reason, the system incorporates multiple levels of redundancy:

- **Primary 132 kV Connection**: Underground line ("Linea SEA") connecting the airport to the public substation CP Malpensa.
- **Secondary 132 kV Connection**: Aerial line providing a redundant HV supply path.
- **Emergency 15 kV Feed**: Additional supply connection from the public MV distributor (E–Distribuzione).

- **Islanding Operation ("Servizio Separato")**: The trigeneration plant can operate autonomously, supplying the entire airport even when fully disconnected from the national electricity grid.

This multilayered redundancy ensures resilience against external disturbances, faults, or upstream contingencies.

3.2.6 Distributed Substation Network

Power is distributed across the airport through a densely interconnected system of medium voltage substations (*Cabine*). These substations support selective protection coordination and sectionalisation. Key categories include:

- **Runway Substations** (e.g., Cabina 1 and 2): Supplying runway and taxiway lighting, signs, and navigation systems.
- **Terminal Substations** (e.g., Cabina 6, 7, 10, 16, 17, 18): Feeding HVAC systems, elevators, IT services, and passenger infrastructures.
- **Cargo Substations** (e.g., Cabina 8 and 25): Serving logistics, cold chain warehouses, and cargo operations.
- **Baggage Handling Substations**: Dedicated to conveyor lines, scanning systems, sorting equipment, and control nodes.

These substations are integrated into a hierarchical protection scheme designed to isolate faults within milliseconds.

3.2.7 Technical and Operational Governance

The operation of the energy system is regulated by a formal **Regolamento di Esercizio**, which defines:

- The roles and responsibilities of SEA as SDC operator,
- The obligations of A2A Airport Energy as plant subconcessionaire,
- The interface rules with Terna and E–Distribuzione,
- Operational protocols for switching, maintenance, protection, and outage management.

The regulatory framework ensures safe operation, compliance with national regulations, and coordination between all actors. Crucially, it mandates automated protection systems capable of isolating faults in extremely short time intervals to prevent cascading failures and ensure uninterrupted airport operations.

For clarity and completeness, the one-line diagram of the Milano Malpensa Airport on-site generation plant is presented in Figure, 3.1. The diagram provides a schematic overview of what is discussed previously, the generation units, the associated steam and gas turbines, the step-up transformers, and the interconnection with the 132 kV high-voltage system. For reasons of confidentiality and security related to critical infrastructure, the representation is intentionally limited to the generation facilities only, while the detailed topology of the medium and low voltage distribution networks is not disclosed in Figures.

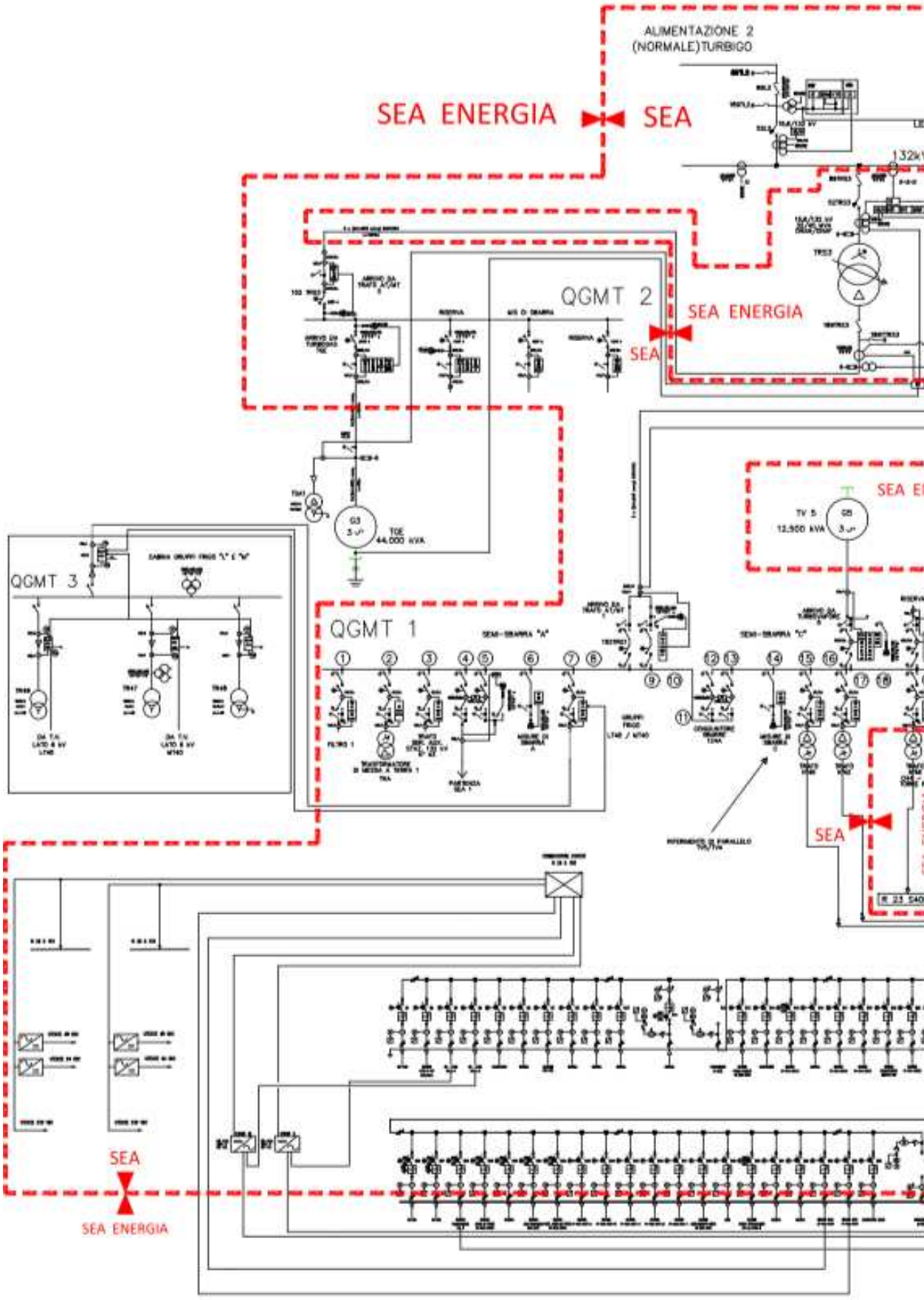

Figure 3.1: MXP Generation Plant (cont.)

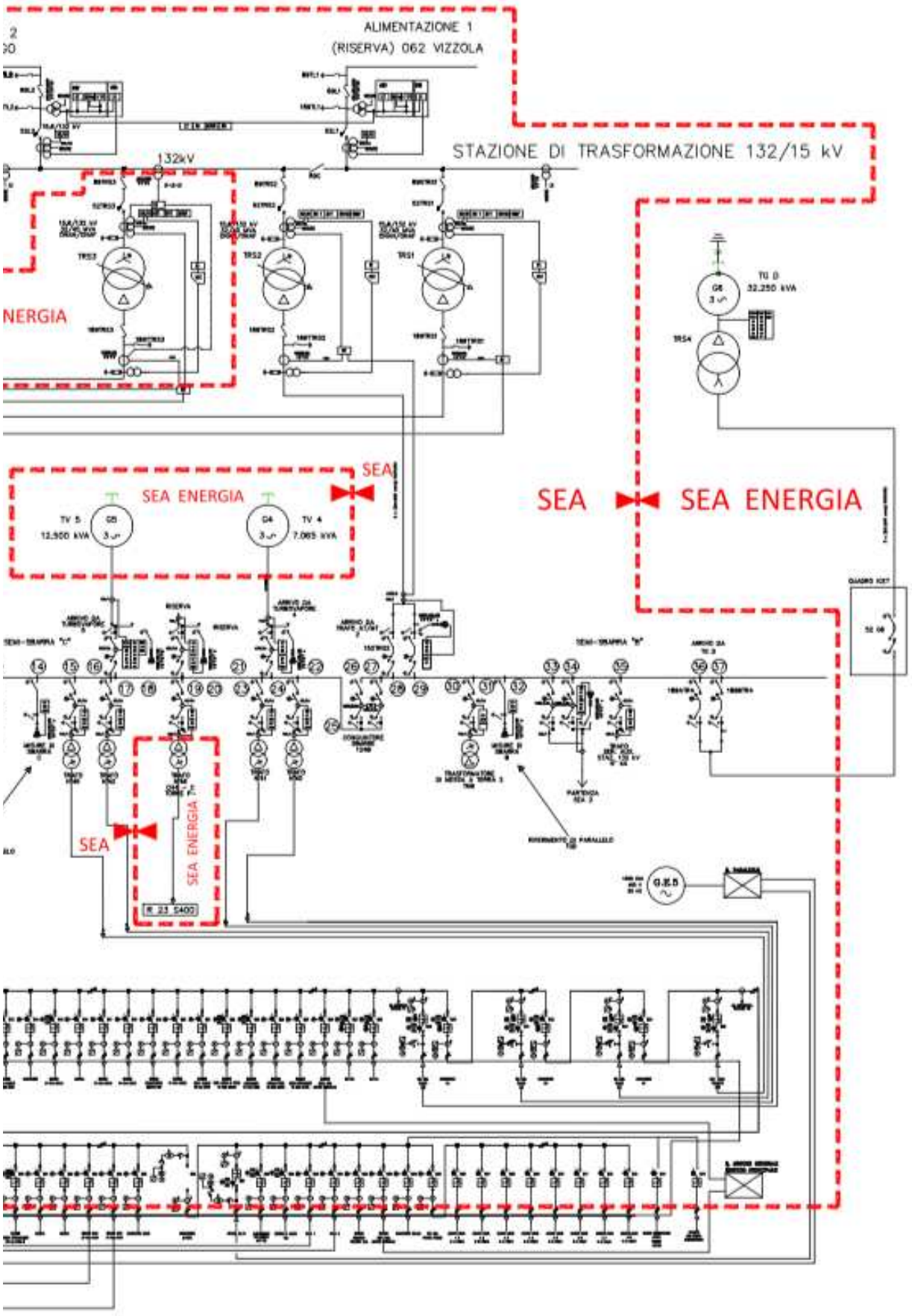

Figure 3.1: MXP Generation Plant (concluded).

3.3 Load Modelling and Network Equivalencing

The airport electrical system supplies a diverse set of loads including runway lighting, navigation systems, HVAC chillers and pumps, conveyor motors, lighting, and auxiliary services. These loads are dispersed across multiple medium voltage (MV) and low voltage (LV) feeders, connected via a hierarchically structured transformer and cable network. Explicitly modelling each downstream element would result in an unnecessarily large dynamic model without improving the accuracy of electromechanical simulations. Instead, a classical network equivalencing strategy is adopted.

3.3.1 Steady-State Based Aggregation

A steady-state load-flow analysis is performed in ETAP to determine the real and reactive power consumption at each MV bus. Following this, all LV loads, feeders, motors, and auxiliary equipment connected downstream of an MV bus are aggregated into a **lumped PQ load**. This PQ representation preserves:

- Active and reactive power demand at the operating point,
- Steady state voltage profile at MV buses,
- Transformer loading conditions,
- Overall power factor.

ETAP automatically determines the equivalent impedance representing the aggregated load, ensuring consistent short-circuit current contribution and reactive power sensitivity.

This approach aligns with established transient stability practices, where the main interest lies in electromechanical time scale behaviour (0.1–10 s), during which load demand is assumed approximately constant [29]. Dynamic load variations typically occur at slower time scales and are outside the scope of rotor angle stability.

3.3.2 Voltage-Dependent Load Representation: ZIP Model

For completeness and to support voltage-sensitivity discussions, the voltage-dependent ZIP model is introduced conceptually. The real and reactive power of a ZIP load are expressed as:

$$P(V) = P_0 \left[a_Z \left(\frac{V}{V_0} \right)^2 + a_I \left(\frac{V}{V_0} \right) + a_P \right], \tag{3.1}$$

$$Q(V) = Q_0 \left[b_Z \left(\frac{V}{V_0} \right)^2 + b_I \left(\frac{V}{V_0} \right) + b_P \right], \tag{3.2}$$

where $a_Z + a_I + a_P = 1$ and $b_Z + b_I + b_P = 1$, with a_Z and b_Z representing constant impedance components, a_I and b_I constant current components, and a_P and b_P constant power components.

Although ZIP models, Figure 3.2, increase accuracy in voltage sensitive studies, the PQ model is sufficient for the electromechanical time scales of transient stability.

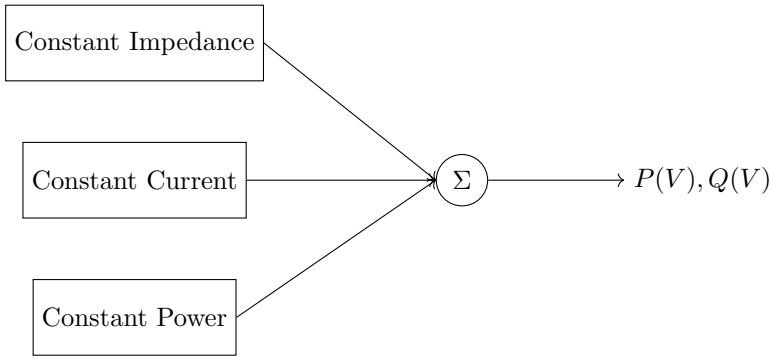

Figure 3.2: Conceptual ZIP load model block diagram.

3.3.3 Modelling of the Induction Machines in the Gruppo Frigo

The Gruppo Frigo at Malpensa Airport includes two high–power induction machines (FRIGO1 and FRIGO2), each driving a large refrigeration compressor used in the chilled water production cycle. These loads are essential for terminal HVAC operation and are classified as strategic elements within the airport's Closed Distribution System (SDC). Their correct representation is therefore important for evaluating the impact of medium voltage disturbances on voltage behaviour, generator stability, and system resiliency.

3.3.3.1 Electrical and Nameplate Parameters

Both machines operate at a rated voltage of 6 kV with a nominal electrical power of approximately 1.492 MW, a rated current of 163 A, a power factor of 0.91, and an efficiency of 96.8%. The locked–rotor current ratio is specified as $I_{\mathrm{lr}}/I_{\mathrm{n}} = 6.0$, corresponding to a starting current of approximately 978 A. The ratio between rotor resistance and magnetising reactance ($R_{\mathrm{w}}/X_{\mathrm{m}} = 0.15$) was also available from the technical documentation.

These parameters were entered into ETAP's nameplate and impedance sections, allowing the software to derive an equivalent electrical representation consistent with a large, high–efficiency compressor motor. Since no manufacturer specific dynamic short–circuit or cage data were provided, default ETAP sequence impedances were retained.

3.3.3.2 Mechanical Load Representation

Refrigeration compressors do not exhibit pump or fan type quadratic torque characteristics. Large HVAC chiller units typically employ centrifugal or screw compressors whose mechanical load increases non-linearly with rotor speed. To reflect this behaviour in steady state and fault studies, the mechanical load associated with FRIGO1 and FRIGO2 was represented using the `COMP CENT` (centrifugal compressor) load characteristic available in ETAP. This curve provides a realistic representation of compressor load dependence on speed and ensures an appropriate active and reactive power demand profile during voltage depressions.

3.3.3.3 Representation in Transient Stability Studies

Due to the limitations of the ETAP student license, detailed induction motor dynamic models (e.g., IM4 or IM5) were not available for transient stability simulations. Consequently, FRIGO1 and FRIGO2 are treated as voltage dependent static loads during transient stability analyses. While this approach does not explicitly model slip, electromagnetic torque, or reacceleration dynamics, it accurately captures the impact of the chiller group on system behaviour through its effects on active power demand, reactive power absorption, and MV bus voltage during and after faults.

The static representation is sufficient for the objectives of this study, which focus on the transient stability of synchronous generators and the overall system response to MV disturbances. The influence of the chiller motors on generator stability is therefore assessed indirectly, through voltage sag severity, load rejection following protection actions, and reactive power redistribution within the network.

3.3.3.4 Implications for later Analysis

Based on the voltage profiles obtained during MV fault simulations, the potential dynamic behaviour of the compressor motors such as torque reduction or risk of stalling is evaluated analytically using well established induction motor characteristics (e.g., torque proportional to the square of terminal voltage). This hybrid approach ensures consistency

between the simulation framework and the physical interpretation of motor behaviour, while remaining fully compatible with the available tool capabilities.

Overall, the adopted modelling strategy provides a reliable and methodologically consistent basis for evaluating generator transient stability, voltage recovery, protection coordination, and resiliency under internal MV fault scenarios involving the Gruppo Frigo subsystem.

3.4 Transmission System and External Grid Representation

The airport is supplied by the regional transmission grid operated by Terna, which has a high short-circuit strength and behaves effectively as an *infinite bus*. Consistent with industry practice and dynamic modelling literature [29], the external grid is represented as a **Thevenin equivalent** voltage source at nominal system frequency and voltage, behind an equivalent short-circuit impedance. This ensures realistic representation of system strength and fault current levels without unnecessary modelling of distant upstream elements.

HV and MV cables within the airport network are represented by their positive sequence impedances, while transformers are modelled using their rated MVA, impedance percentage, and tap positions. Electromagnetic transient phenomena (e.g., saturation, frequency-dependent impedance, ferroresonance) are not included, as ETAP's transient stability engine operates on phasor domain electromechanical time-scales and is not intended for EMT analysis.

3.5 Synchronous Generator Modelling

Synchronous generators constitute the dominant dynamic elements influencing transient stability in conventional power systems. They provide inertia, synchronizing torque, damping torque, reactive power support, and frequency regulation. For this reason, their mathematical representation must accurately capture both electromagnetic and electromechanical phenomena under normal as well as disturbed operating conditions. The modelling approach adopted in this study follows the principles outlined in Kundur [29] and the IEEE Guide for Synchronous Generator Modelling Practices [26].

The generation units considered in this study are representative of medium scale

synchronous machines interfaced with the airport electrical network. These units are equipped with brushless excitation systems and conventional speed-governing mechanisms. Compared to large utility-scale steam or hydro generators, such machines typically exhibit lower inertia constants, making them more sensitive to rotor-angle deviations during transient disturbances. Consequently, accurate modelling of subtransient dynamics and excitation control systems is essential for a reliable assessment of system stability margins.

3.5.1 Machine Model Structure

Each synchronous generator is represented using the standard **subtransient model** in the dq reference frame. This model captures the rapid decay of rotor flux linkages following the application or removal of fault currents. The key electrical components represented include:

- **Stator windings** in the d–q reference frame;
- **Field winding** on the d-axis;
- **Damper (amortisseur) windings** on both d- and q-axes.

These elements allow the generator to produce subtransient, transient, and steady state reactances, denoted respectively as X''_d, X'_d, and X_d on the d-axis (and similarly X''_q, X'_q, X_q for the q-axis). The subtransient reactances determine the initial short-circuit current injection and strongly influence post-fault voltage recovery.

A conceptual diagram of the dq-axis equivalent is shown in Fig. 3.3.

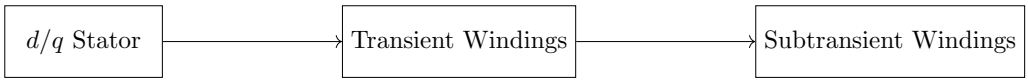

Figure 3.3: Conceptual dq-axis model of a synchronous generator (simplified).

3.5.2 Mechanical Dynamics and Swing Equation

The electromechanical dynamics of the generator rotor are governed by the classical swing equation [29]:

$$\frac{2H}{\omega_s}\frac{d^2\delta}{dt^2} = P_m - P_e - D\frac{d\delta}{dt}, \tag{3.3}$$

where:

- H is the per-unit inertia constant (s),
- ω_s is synchronous speed,
- δ is the rotor electrical angle relative to the infinite bus,
- P_m is the mechanical input power,
- P_e is the electrical air-gap power,
- D is the damping coefficient.

During a fault, P_e drops sharply due to reduced terminal voltage, causing the rotor to accelerate. The magnitude and duration of this acceleration depend on the fault severity and clearing time. For generators with small inertia, the rate of change of rotor angle can be substantial, reducing the system's tolerance to delayed protection clearing.

3.5.3 Excitation System Modelling

The voltage regulator strongly influences post-fault voltage recovery, reactive power support, and system damping. In this study, each generator is equipped with a standard brushless exciter following the AVR structure recommended in IEEE machine models [26]. The AVR includes:

- A voltage measurement transducer;
- A PI-type regulator;
- Field voltage limits (ceiling and floor);
- Gain limits and rate limiters.

The simplified AVR equation is:

$$V_{fd}(t) = \text{clip}[K_A\,(V_{\text{ref}} - V_t(t))]_{V_{\min}}^{V_{\max}}, \tag{3.4}$$

where $V_t(t)$ is terminal voltage magnitude and K_A is the regulator gain. High-gain AVRs typically improve transient voltage performance but may reduce damping if not paired with a stabilizing signal. The AVR internal control loop constants (KA, TA, TE, KF, etc.) are not disclosed in the technical documentation of the Malpensa trigeneration plant, as they fall under protected operational parameters regulated by SEA and Terna. Therefore, a standard IEEE AC5A exciter model was adopted with representative

parameters aligned with typical medium-scale synchronous generators. The functional behaviour specified in the grid code ($\cos\varphi$ control, voltage limits, reactive support) is preserved, ensuring that the model reflects the real plant capabilities.

3.5.4 Turbine Governor Modelling

The mechanical input power P_m of each synchronous generator is regulated by the turbine-governor system. For the generating units considered in this study, a simplified first-order droop model is adopted:

$$P_m(s) = \frac{1}{1 + sT_g}\left[P_{\text{ref}} - \frac{1}{R}\Delta f(s)\right], \tag{3.5}$$

where R denotes the droop coefficient and T_g the equivalent governor time constant. This representation is adequate for transient-stability simulations focused on short-circuit disturbances, since the mechanical power does not vary significantly during the fault interval itself. The governor action mainly affects the post-fault recovery phase rather than the immediate fault-on response.

3.5.5 Power System Stabilizer (PSS)

To enhance damping of electromechanical oscillations, some generators may include a Power System Stabilizer (PSS). Although not active in all generators at the airport, PSS modelling follows the standard structure:

- Washout filter,
- Lead–lag compensator stages,
- Gain limiter,
- Stabilizing signal injection into the AVR summing junction.

The PSS produces a stabilizing torque proportional to rotor speed deviation, improving small-signal damping and preventing oscillatory instability following faults.

3.5.6 Parameter Selection and ETAP Implementation

The generator parameters used in simulations (reactances, time constants, inertia values, AVR gains, governor parameters) are taken either from manufacturer datasheets or typi-

cal values for steam and gas generating sets when detailed data are unavailable. ETAP's library of IEEE-standard machine models facilitates the direct implementation of:

- Subtransient synchronous machine models,
- IEEE-type excitation systems (EXST, ESAC, etc.),
- Standard steam and gas turbine governor models (e.g., TGOV1 or equivalent).

The integration of these models ensures that crucial transient behaviours fault current injection, voltage recovery, frequency deviation, rotor acceleration, and damping are all realistically captured.

3.6 Photovoltaic Plant Modelling

The Malpensa Airport electrical system incorporates a 10 MW AC photovoltaic (PV) plant connected at the medium-voltage (MV) level. Unlike synchronous machines, PV resources interface with the grid through power electronic inverters, which behave fundamentally differently during normal operation and grid disturbances. Their dynamic response is governed primarily by control-loop design, current limitation behaviour, and Low-Voltage Ride-Through (LVRT) requirements, rather than by electromechanical motion. As a result, a modelling framework must accurately represent both the electrical characteristics of the PV array and the dynamic behaviour of the inverter.

The modelling developed in this work combines a detailed calculation of the PV array configuration with an aggregated inverter representation suitable for MV transient stability simulations. This approach reflects best engineering practice for system-level stability studies, where the internal electrical topology of a PV plant is typically abstracted into a single equivalent generator [1, 23].

3.6.1 PV Array Electrical Design and Module Parameters

The PV plant employs utility-scale monocrystalline silicon modules rated at 550 W under Standard Test Conditions (STC), corresponding to a solar irradiance of 1000 W/m^2, a cell temperature of 25 °C, and an air mass (AM) of 1.5. The key module parameters used for array configuration are:

$$V_{mp} = 42.76 \text{ V},$$

$$V_{oc,STC} = 50.13 \text{ V},$$

$$\beta_{Voc} = -0.2685\%/^{\circ}\text{C}.$$

Modern large scale PV installations use a 1500 V DC architecture to reduce current, cable cross-sections, power losses, and BOS (Balance-of-System) costs. To ensure that strings remain within this limit even at low temperatures, a cold-temperature correction must be applied. The open-circuit voltage at temperature T is:

$$V_{oc}(T) = V_{oc,STC}\left[1 + |\beta_{Voc}|(25 - T)\right]. \tag{3.6}$$

Assuming a conservative minimum ambient temperature typical for northern Italy, the maximum number of modules in series is:

$$N_{s,\max} = \left\lfloor \frac{1500}{V_{oc}(T_{\min})} \right\rfloor = 27. \tag{3.7}$$

The corresponding maximum power point (MPP) string voltage is:

$$V_{\text{string,mp}} = 27 \times V_{mp} \approx 1155 \text{ V}, \tag{3.8}$$

which lies comfortably within the MPP tracking range of commercial 1500 V inverters.

3.6.2 Array Sizing and DC/AC Ratio

To achieve a 10 MW AC output at the point of interconnection (POI), the PV plant is oversized on the DC side a common practice to improve inverter utilisation and annual energy production. The DC/AC ratio chosen is approximately 1.2, leading to:

$$P_{\text{dc,total}} \approx 12 \text{ MW}_{\text{dc}}. \tag{3.9}$$

The total number of PV modules required is then:

$$N_{\text{total}} = \frac{P_{\text{dc,total}}}{P_m} \approx \frac{12 \times 10^6}{550} \approx 21{,}800 units. \tag{3.10}$$

With 27 modules per string, this yields:

$$N_{\text{strings}} = \frac{21{,}800}{27} \approx 807 \text{ strings.} \tag{3.11}$$

These values align with modern utility scale PV system design practices.

3.6.3 Aggregated Inverter Model

For the purposes of system level transient stability analysis, the detailed DC-side structure of the photovoltaic (PV) plant (strings, combiners, DC feeders, and low-voltage transformers) is abstracted into a single **aggregated grid-following inverter** connected to the 15 kV medium-voltage bus.

The aggregated inverter is characterised by:

- A rated active power of 10 MW,
- An apparent power rating of approximately 11.1 MVA,
- Reactive power capability compatible with a ± 0.9 power factor,
- Unity power factor in normal operating conditions, with optional reactive dispatch for sensitivity studies.

Figure 3.4 presents the simplified block representation used in ETAP.

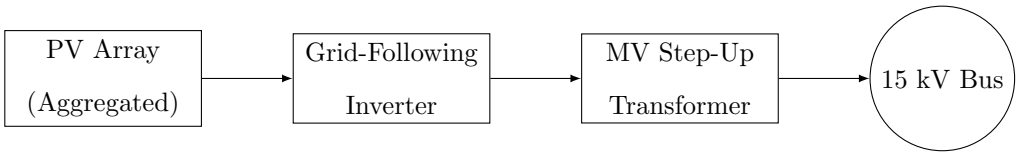

Figure 3.4: Aggregated PV plant representation adopted in ETAP.

3.6.4 Grid-Following Inverter Dynamics

The PV system is modelled as a **grid-following inverter**, synchronising to the grid voltage via a Phase-Locked Loop (PLL). Internally, such inverters operate with multi-layered control loops:

- **Inner current controllers**, which regulate the dq-axis currents and enforce semiconductor current limits.
- **Outer active/reactive power control**, which maintains setpoints for P and Q during steady-state.

- **DC-link control**, which adjusts active-power extraction from the PV array to maintain the DC bus voltage.
- **Current limiting during disturbances**, typically restricting fault current to 1.1–1.3 p.u.

These control loops operate at sub-millisecond time scales and are not explicitly represented in ETAP's electromechanical transient stability models. Instead, ETAP uses RMS-based inverter models that enforce:

- Active and reactive power limits,
- Short-circuit current limits,
- Grid-following synchronisation,
- And voltage-dependent reactive current support during faults (Fault Ride-Through behaviour).

3.6.5 Fault Ride-Through (FRT) and Low-Voltage Behaviour

Modern grid codes (e.g., CEI 0-16, ENTSO-E) require inverter-based resources to provide voltage support during short-duration voltage depressions. While full Low Voltage Ride Through (LVRT) capability is normally defined through a time-dependent voltage envelope, The ETAP inverter model employed in this study does **not** implement an explicit voltage time LVRT tripping curve. Instead, the model provides **Fault Ride-Through (FRT) reactive current injection**, which governs the inverter's behaviour during voltage sags. The main FRT features available and used in this thesis are:

- **Voltage-dependent reactive current injection**: when the terminal voltage drops below predefined thresholds (dead-band limits), the inverter injects reactive current according to the slope coefficients K_1 and K_2.
- **Short-circuit current limitation**: the inverter's current output is constrained between $I_{\text{sc,min}}$ and $I_{\text{sc,max}}$, typically in the 1.1–1.3 p.u. range.
- **No automatic LVRT tripping**: because the voltage time envelope and undervoltage (27) protection blocks are not part of this model, the inverter does not autonomously disconnect when the voltage remains below a threshold for an extended period.

- **Manual tripping when required**: to emulate realistic LVRT violations (e.g., prolonged voltages below 0.2–0.3 p.u represented in Figure 3.5), the inverter is deliberately disconnected through a time tagged event in the simulation.

This modelling approach captures the essential dynamic characteristics of PV inverters during grid faults (namely reactive current support and limited short-circuit contribution) while acknowledging the limitations of the available dynamic model.

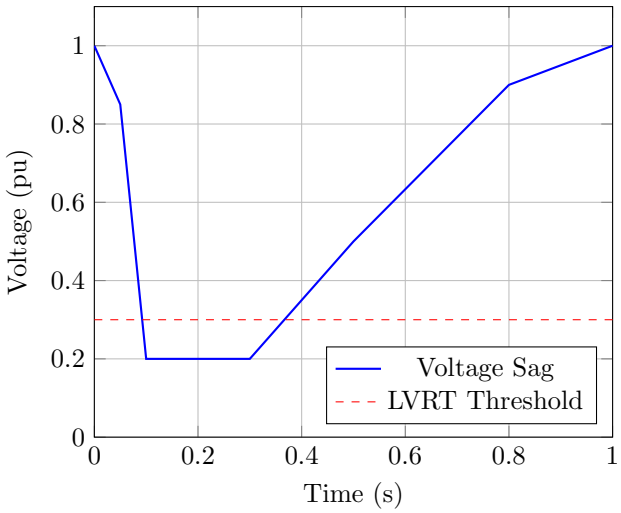

Figure 3.5: Illustrative LVRT as a *reference criterion* to emulate realistic behaviour in accordance with CEI 0-16 and ENTSO-E requirements.

3.6.6 Suitability of the Aggregated PV Model for Stability Studies

Inverter-based resources do not contribute inertia and therefore do not directly influence rotor-angle stability. Their impact on transient stability arises from:

- Their limited contribution to fault current,
- Voltage support through reactive current injection during FRT operation,
- Post-fault active power restoration,
- Potential disconnection during severe or long-duration voltage depressions (emulated manually).

Although the ETAP model used does not include a full LVRT voltage time envelope, it provides sufficient fidelity to represent the interaction between the PV system and the medium voltage network during faults. It therefore supports the objectives of this

thesis, which include evaluating voltage recovery, protection coordination, and generator stability margins under various disturbance scenarios.

3.7 Protection Modelling

Protection systems play a decisive role in determining the electromechanical response of a power system during and after a disturbance. The duration of a fault, the selectivity of tripping, and the type of protection elements that operate all directly influence the generator rotor acceleration, voltage depression, and post-fault stability. For this reason, realistic modelling of fault-clearing times and protection behaviour is essential for meaningful transient stability analysis [29].

The protection modelling used in this thesis focuses on four core aspects:

1. Representation of realistic HV and MV circuit-breaker clearing times.
2. Modelling of overcurrent protection functions (50/51/51V) and their impact on clearing behaviour.
3. Representation of directional and differential protection for selective isolation.
4. Construction of a logical generator-tripping scheme that reflects actual protection device behaviour.

This section provides a comprehensive description of these modelling components and their integration into ETAP's transient stability simulations.

3.7.1 Circuit Breaker Clearing Times

Fault-clearing time is the sum of:

- The **relay operating time**, and
- The **breaker mechanical opening time**.

Based on industrial data and site-specific information, the following clearing times were adopted:

$$\text{HV breaker clearing time} \approx 40 \text{ ms (mechanical)} + 20 \text{ ms (protection inertia)} = 60 \text{ ms}, \tag{3.12}$$

$$\text{MV breaker clearing time} \approx 60 \text{ ms (mechanical)} + 20 \text{ ms (protection inertia)} = 80 \text{ ms}. \tag{3.13}$$

These times align with modern vacuum and SF_6 breaker performance characteristics typically found in 15 kV systems. Backup clearing is set to approximately 300 ms to reflect the coordinated operation of time-overcurrent relays.

3.7.2 Overcurrent Protection Functions

The principal protection functions that influence clearing times in transient stability simulations are:

Instantaneous Overcurrent (50). This element trips without intentional delay when current exceeds a high threshold. Although called "instantaneous," actual operation includes the breaker's mechanical delay. In the present model, this corresponds to the adopted 60–80 ms clearing interval.

Time-Overcurrent (51). The 51 function provides backup protection through a time inverse characteristic. For faults that do not exceed the 50 pickup level, 51 dictates the clearing time. Typical operation in this study ranges from 0.20 to 0.30 s, depending on relay grading.

Voltage-Restrained Overcurrent (51V). Close-in faults near generators produce deep terminal voltage sags before overcurrent elements detect high current. The 51V function adjusts the pickup level based on measured voltage. This ensures dependable tripping even under depressed voltage. Its presence is crucial for accurately determining generator-side clearing times.

3.7.3 Inverse-Time Overcurrent Characteristics

Industrial protection schemes typically follow IEC-type inverse-time characteristics. The general inverse-time model is:

$$t = \frac{K}{\left(\frac{I}{I_p}\right)^{\alpha} - 1}, \tag{3.14}$$

where:

- I is the fault current,
- I_p is the relay pickup current,
- K and α define the curve type (standard inverse, very inverse, extremely inverse).

A graphical illustration of typical coordination curves is shown in Fig. 3.6.

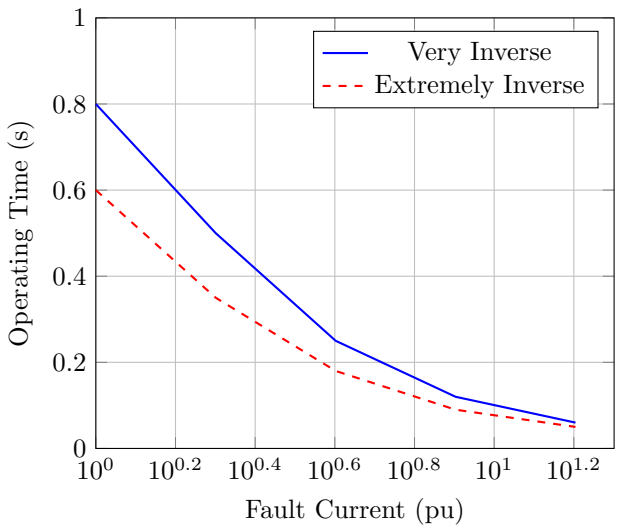

Figure 3.6: Illustrative IEC IDMT coordination curves used in MV feeder protection.

These curves determine the relative selectivity (only the nearest device trips) between upstream and downstream relays.

3.7.4 Directional Overcurrent Protection (67)

The airport MV system contains multiple feeders in interconnected arrangements. Directional protection functions are therefore necessary to avoid unnecessary tripping of healthy feeders.

A directional overcurrent relay uses the power-angle or current-angle relationship to determine fault direction, operating only if the fault is within its forward zone. This ensures selectivity in systems with parallel feeders or ring configurations.

3.7.5 Differential Protection (87)

Differential protection is applied to generators, transformer banks, and critical bus sections. The 87 function compares currents entering and leaving the protected zone:

$$\sum I_{\text{in}} = \sum I_{\text{out}}. \tag{3.15}$$

A significant mismatch indicates an internal fault. Operating times for differential protection are typically the fastest among all protection types (20–40 ms), and in this study they are modelled as **immediate tripping**.

3.7.6 Synchronism Check Protection (25)

The synchronism check function (ANSI 25) supervises circuit breaker closing operations by verifying acceptable phase-angle, frequency, and voltage differences between two electrical systems prior to re-energisation. This protection is particularly relevant during reclosing sequences following fault clearance, grid restoration, or transitions between islanded and grid-connected operation.

In the context of this study, the ANSI 25 function does not directly influence fault clearing times or transient stability margins, as breaker reclosing actions were not modelled dynamically. However, its presence is acknowledged in the protection summary because it governs the permissibility of post-fault reconnection of generators or network sections. The synchronism check logic ensures that reclosing does not occur under conditions that could result in severe electromechanical stress or loss of synchronism.

Accordingly, ANSI 25 is represented implicitly through operational assumptions rather than through time-domain relay logic, and its monitored variables such as frequency difference (Δf), voltage difference (ΔV), and phase-angle displacement ($\Delta\delta$) are evaluated qualitatively from the simulated post-fault responses.

3.7.7 Thermal Protection (49)

Thermal protection (ANSI 49) is designed to prevent excessive heating of electrical equipment by monitoring the cumulative thermal effect of current over time, typically through an I^2t-based model. This function is essential for protecting generators, transformers, and cables against prolonged overloads or sustained abnormal operating conditions.

In transient stability studies, however, the time scale of interest is generally limited to short-duration disturbances on the order of several hundred milliseconds to a few seconds. As a result, thermal limits are not approached during the simulated fault events considered in this work. Consequently, ANSI 49 does not contribute to fault clearing decisions within the transient simulations and is therefore modelled as an alarm-only function.

Its inclusion in the protection summary table reflects completeness of the protection

scheme rather than active involvement in transient fault isolation. The relevant observed variable for ANSI 49 remains the RMS current magnitude, which is examined to confirm that no abnormal thermal accumulation occurs during the studied disturbances.

3.7.8 Representation of Protection in Transient Stability Simulations

ETAP transient stability simulations do not execute detailed relay logic unless the protection and coordination modules are explicitly enabled. Since faults were introduced manually in this study, each protection function is represented through:

- Assigned clearing times for each relay type,
- Selective breaker operations in the event sequence,
- Inferred tripping behaviour from fault currents and voltages.

This approach ensures credible clearing times and realistic relay behaviour without requiring full logical relay simulation.

3.7.9 Protection Function Summary Table

Table 3.1: Protection functions and representation in transient stability simulations.

Function	**Purpose**	**Representation**	**Observed Variables**
50 (IOC)	Fast tripping for close-in faults	Clearing in 60–80 ms	i_{fault}, rotor angle
51 (TOC)	Time-coordinated backup	0.20–0.30 s clearing	Voltage sag, P_e, δ
51V	Voltage-restrained OC	Reduced time under deep sag	V_t, torque
67	Directional OC	Selective feeder isolation	Current angle, topology
25	Synch-check	Reclosing logic	Δf, ΔV
49	Thermal protection	Alarm-only	RMS current
87	Differential	Instantaneous clearing	Differential current

3.7.10 Generator Tripping Logic

To realistically model generator disconnection, a hierarchical tripping logic was adopted:

1. **Internal generator-zone faults** (87G/87T) → immediate trip.
2. **Severe terminal voltage collapse** ($V_t < 0.3$–0.4 pu, sustained) → trip via equivalent 51V.
3. **Loss of synchronism** (unbounded $\delta(t)$ growth after clearing) → trip via conceptual 78.
4. **Feeder isolation** (breaker opens the generator feeder) → generator removed unless explicitly islanded.
5. **Otherwise**, the generator remains online.

The logical flow is shown in Fig. 3.7.

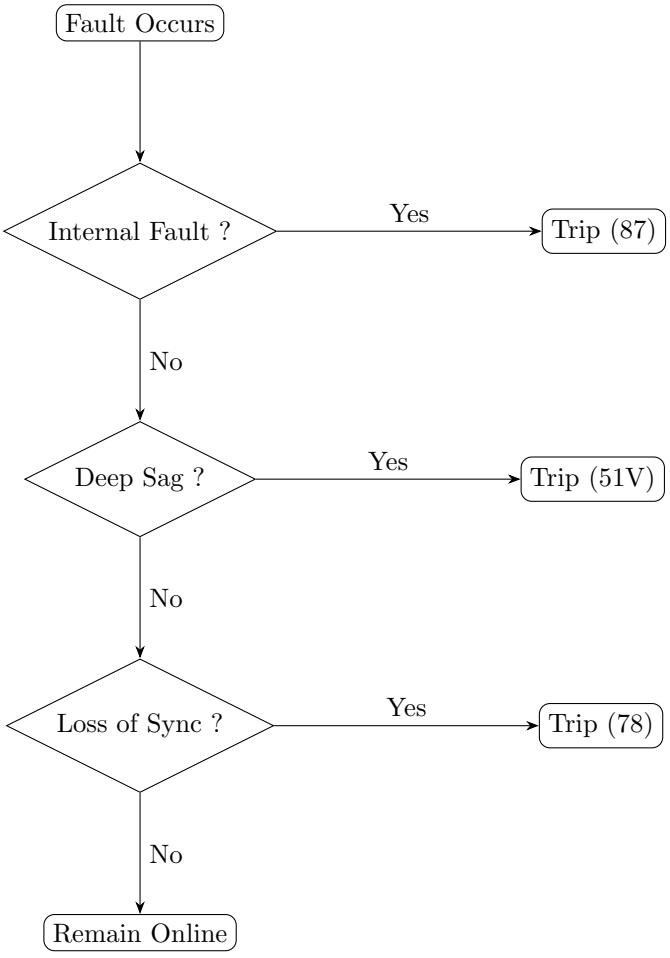

Figure 3.7: Generator tripping logic used in the modelling.

3.8 PV Behaviour During Faults

The behaviour of photovoltaic inverters during grid faults differs fundamentally from that of synchronous generators. PV inverters are power electronic devices whose short-circuit current, synchronization, and voltage support capabilities are governed by their control algorithms rather than electromechanical dynamics. Their treatment in transient stability studies must therefore reflect their inherent limitations and control based behaviour rather than classical machine physics [23].

3.8.1 Fault Current Characteristics

Unlike synchronous generators, which can contribute several multiples of rated current during subtransient intervals, grid following PV inverters intentionally limit their current injection to protect their semiconductor devices. Most commercial inverters cap the peak fault current to approximately 1.1–1.3 p.u. of rated current for one or two cycles, after which internal current limiting controls become active. This behaviour is reproduced in the ETAP inverter model through the "Short-Circuit Current Limit" block, which constrains the inverter current between $I_{\mathrm{sc,min}}$ and $I_{\mathrm{sc,max}}$ as a function of terminal voltage.

Two important consequences follow:

1. **PV inverters do not materially drive upstream protection**. The limited current contribution is insufficient to operate phase or earth fault overcurrent elements on MV feeders.

2. **The breaker clearing the fault is always the device electrically closest to the fault**. The PV feeder breaker does not trip in response to upstream disturbances unless a dedicated undervoltage or internal protection criterion is violated.

As a result, the PV plant behaves as a current limited device during faults, with synchronous generators and the external grid dominating fault current dynamics.

3.8.2 Breaker Operation in the Presence of PV

Because the inverter behaves as a limited current source, it cannot affect the operation of upstream MV protection. Consequently:

- The breaker nearest to the fault always clears the disturbance,

- The PV feeder breaker opens only if a local undervoltage condition is manually imposed or an internal inverter fault occurs,
- FRT behaviour ensures that the inverter *remains connected* during short sags created by normal MV breaker operations.

Therefore, the presence of the PV inverter does not compromise protection selectivity on the medium-voltage network.

3.8.3 Impact of PV Disconnection on System Stability

If a severe and sustained voltage sag violates realistic LVRT criteria (as interpreted from the reference envelope), the PV inverter is disconnected via a scheduled event. In the Malpensa system:

- The PV plant contributes 10 MW relative to a significantly larger combined synchronous generation portfolio,
- The inverter provides no inertia and only limited reactive support,
- Its disconnection does not compromise rotor-angle stability of synchronous generators.

Thus, PV loss during extreme disturbances has a negligible impact on overall transient stability, although it may slightly influence post-fault voltage recovery when operating near feeder voltage limits.

3.9 Island Mode Operation (Servizio Separato)

The Milano Malpensa Airport energy system is equipped with the capability to operate in *island mode* (also referred to as *funzionamento in isola* or *servizio separato*), a critical operational state in which the airport's Closed Distribution System (SDC) is electrically separated from the national public grid. This mode guarantees the continuity of power supply during external disturbances, ensuring that airport operations remain fully functional even in the event of a widespread blackout.

Island operation involves a coordinated sequence of protection actions, dynamic transitions, and regulatory controls that must be correctly executed by both the generation units and the distribution system operator (SEA). The following subsections provide a detailed overview of the islanding process and associated procedures.

3.9.1 Transition to Island Mode and Transient Management

A transition to island mode is triggered when a disturbance or fault occurs on the public grid typically involving the 132 kV interconnection in the case of Malpensa. When the external fault is detected, protection devices automatically initiate the disconnection of the airport's SDC from the national network by opening the relevant high voltage switches.

Following this disconnection, the internal Trigeneration units must withstand the resulting *elettrodinamico transitorio* (electrodynamic transient), which includes:

- A sudden change in electrical load,
- An abrupt shift in frequency and voltage,
- The loss of the external grid as an infinite bus reference.

To maintain continuity of supply, the Trigeneration must remain online and stabilize the SDC autonomously immediately after separation.

3.9.2 Frequency and Voltage Regulation During Island Operation

Once the system has successfully islanded, the generation plant becomes the sole reference for all key electrical parameters of the airport grid. Synchronous generators must therefore assume *master control* of frequency and voltage.

Frequency Regulation

The system must remain within stringent frequency limits, ± 0.5 Hz deviation from the nominal 50 Hz in steady state, and within ± 1 Hz during transient load changes or switching. These requirements ensure the stable operation of airport loads and sensitive equipment, including navigation systems, baggage handling plants, and airfield lighting.

Voltage Regulation

Voltage regulation in island mode is achieved by the generators' automatic voltage regulators (AVRs), which maintain terminal voltage within prescribed limits. Additional voltage adjustments may occur through:

- Automatic tap-changing transformers,

- Semi-automatic control actions executed by the system operator,
- Coordinated dispatching of reactive power.

Together, these mechanisms ensure that the entire SDC maintains adequate voltage levels despite load variations and generator operating conditions.

3.9.3 Failure of Islanding and Manual Voltage Restoration

If the internal generation units are unable to survive the initial transient following separation, resulting in a collapse of frequency or voltage, the system enters the state known as *mancata isola* (failed islanding). In this condition, the SDC becomes de-energized, producing a local blackout within the airport.

When this occurs, the Producer must perform a manual *rilancio di tensione* (voltage restoration), which involves:

- Reclosing the 132 kV connection switches,
- Verifying, in coordination with the Distributor (SEA), that no emergency generators are operating on the de-energized portion of the network,
- Restoring the SDC to a normal energized state before proceeding with generator re-synchronization or load reconnection.

This procedure ensures that no unintended parallel operation or unsafe energization occurs during restoration.

3.9.4 Total Blackout and Black Start Capability

In the rare event of a total blackout where both the public grid and the main generation units are unavailable the airport system initiates a *Black Start* procedure. Under SEA's instruction, the Producer may employ dedicated emergency generators (for example, unit G5 at Malpensa) to supply the initial power required to restart:

- Essential auxiliary systems,
- The main gas turbines,
- The internal SDC infrastructure.

This emergency generator must **never** be operated in parallel with the national grid unless explicitly authorized by the Distributor. Its exclusive purpose in this context is to bootstrap the trigeneration plant when no other supply source is present.

3.9.5 Re-synchronization with the National Grid

Once the national grid has been restored and external conditions are stable, the airport must transition from island mode back to normal parallel operation. This process requires a controlled **re-synchronization** procedure, executed using dedicated synchronization relays (e.g., device 25A). The synchronizer ensures alignment of:

- Frequency,
- Voltage magnitude,
- Phase angle

between the airport island and the national grid before any circuit breaker is reclosed.

A crucial requirement is that all emergency generators used during the blackout must be shut down prior to the parallel reconnection maneuver to avoid unintended parallelism. Once synchronization is validated, the HV switches are closed and the system transitions back into normal grid-connected SDC operation.

3.10 Black Start Procedure (Riaccensione Programmata)

In the operational framework of the Milano Malpensa, the *Black Start* (*riaccensione programmata*) represents a critical emergency procedure designed to restore power to the Closed Distribution System (SDC) following a complete electrical blackout. This condition occurs when both the national public grid and the airport's internal primary generation units are simultaneously unavailable, resulting in a fully de-energized SDC incapable of performing an automatic transition to island mode.

The Black Start procedure is therefore an essential component of the airport's resilience strategy and must be executed with strict coordination between the Distributor (SEA) and the Producer (A2A Airport Energy).

3.10.1 Trigger Conditions

A Black Start is initiated exclusively when the following conditions are simultaneously met:

- The national public distribution grid supplying the airport is unavailable, and

- The airport's internal generation units (cogenerators) have failed to remain online, resulting in *mancata isola* (failed islanding).

Under these circumstances, the entire SDC is de-energized and cannot rely on internal inertia or residual voltage to restart the cogeneration units. A controlled Black Start maneuver must therefore be executed.

3.10.2 Use of Emergency Generators

The core of the Black Start procedure relies on the controlled use of dedicated emergency generators owned by the Producer. These units provide the initial power required to reactivate plant auxiliaries and bring the main generation units back online.

The designated generators is emergency generator G5 with its steam turbine TV5.

Their operational constraints are strict:

- Under normal conditions, these emergency units are **prohibited** from operating in parallel with the Distributor's grid;
- They may only be connected to the SDC during a Black Start or when explicit authorization is granted by the Distributor.

This ensures compliance with safety regulations and prevents unintended parallel operation during grid energization.

3.10.3 Transition to Normal Operation

Once the emergency generators have supplied sufficient power to restart the cogeneration plant's auxiliaries, the main generation units can be brought back online. After the internal production capacity is restored, the emergency generator must be disconnected.

Before performing a re-synchronization maneuver with the national grid:

- All emergency generators used during the Black Start must be shut down,
- The SDC must be stabilized in island mode,
- Frequency and voltage must be restored to nominal operating limits.

Only after these conditions are met can a controlled re-synchronization with the public grid be performed.

3.11 Distinction Between Island Mode and Black Start

Although both island mode and Black Start procedures concern the operation of the airport under abnormal grid conditions, they represent fundamentally different states and must not be confused.

3.11.1 Island Mode (Funzionamento in Isola)

Island mode occurs when:

- The airport becomes disconnected from the national grid due to an external disturbance, **but**
- The internal cogeneration units **remain online** and successfully absorb the electrodynamic transient.

In this state, the SDC remains energized and the cogenerators assume full responsibility for:

- Frequency regulation,
- Voltage control,
- Load balancing.

If the internal generation survives the transient, the airport continues operating independently without service interruption.

3.11.2 Black Start

Black Start is fundamentally different. It is triggered only when:

- Both the public grid and the internal generation units are unavailable,
- The transition to island mode fails (*mancata isola*),
- The SDC is completely de-energized.

In such a scenario, the Black Start provides a recovery mechanism using an emergency generator to power essential auxiliaries and restart the cogenerators.

3.11.3 Functional Relationship

The relationship between island mode and Black Start can be summarized as follows:

- A Black Start is **not** a form of island mode.
- Black Start is an **emergency recovery action** used to enable the system to eventually return to islanded operation after a total blackout.
- Island mode is an **operational state**, whereas Black Start is a **procedure**.

Thus, while island mode is the preferred outcome following a grid failure, Black Start is the contingency process used to restore islanding capability when internal generation collapses.

3.12 Conclusion

This chapter has presented a complete modelling framework for the transient stability analysis of the Malpensa Airport electrical system. Detailed synchronous generator models, aggregated load models, accurate PV system representation, realistic fault formulations, and comprehensive protection modelling have been developed in accordance with established stability analysis methodologies [29, 26].

The modelling approach captures:

- Electromechanical response of turbo gas and steam turbine generators,
- Voltage regulation and frequency control through AVR and governor systems,
- PV array sizing and inverter-based grid-following behaviour,
- Realistic clearing times for HV/MV breakers,
- Protection elements such as 50, 51, 51V, 67, and 87,
- Generator tripping logic for internal faults, deep voltage collapses, loss of synchronism, and feeder isolation,
- And the passive, current-limited behaviour of PV resources during faults.

These models collectively form the analytical foundation for evaluating critical clearing times, generator synchronism, and post-fault voltage recovery under various disturbance scenarios.

Summary of Modelling Solutions Adopted

To ensure the modelling was both accurate and computationally efficient, the following solutions were implemented:

1. **Network Equivalencing**: LV networks and feeder loads were aggregated into lumped PQ loads at MV buses to reduce model complexity while preserving power flow characteristics.

2. **Detailed Generator Modelling**: IEEE subtransient synchronous machine models with AVR and governor systems were implemented to accurately reproduce short-term electromechanical behaviour.

3. **PV Plant Aggregation**: The 12 MW_{dc} PV plant was modelled as a single 10 MW grid-following inverter connected to the 15 kV bus, reflecting system-level stability requirements.

4. **Realistic Clearing Times**: HV and MV breaker clearing times were modelled as 60 ms and 80 ms respectively, with a 300 ms backup delay.

5. **Protection Mapping**: Overcurrent, directional, and differential functions were mapped to equivalent clearing times because ETAP transient stability does not directly run relay logic during manual event simulations.

6. **Generator Tripping Logic**: A hierarchical scheme was developed to determine whether generators should disconnect following internal faults, severe voltage sags, loss of synchronism, or feeder isolation.

7. **FRT-Based PV Behaviour**: During voltage sags, the inverter remains connected and provides voltage-dependent reactive current injection according to its Fault Ride-Through (FRT) settings, while ignoring sub-cycle micro-dips due to RMS filtering.

These modelling decisions ensure that the simulation results presented in subsequent chapters reflect the actual operating characteristics and constraints of the Malpensa Airport electrical system. Figure 3.8 presents the final ETAP representation of the airport generation module, incorporating all the modelling assumptions and simplifications discussed in the previous sections.

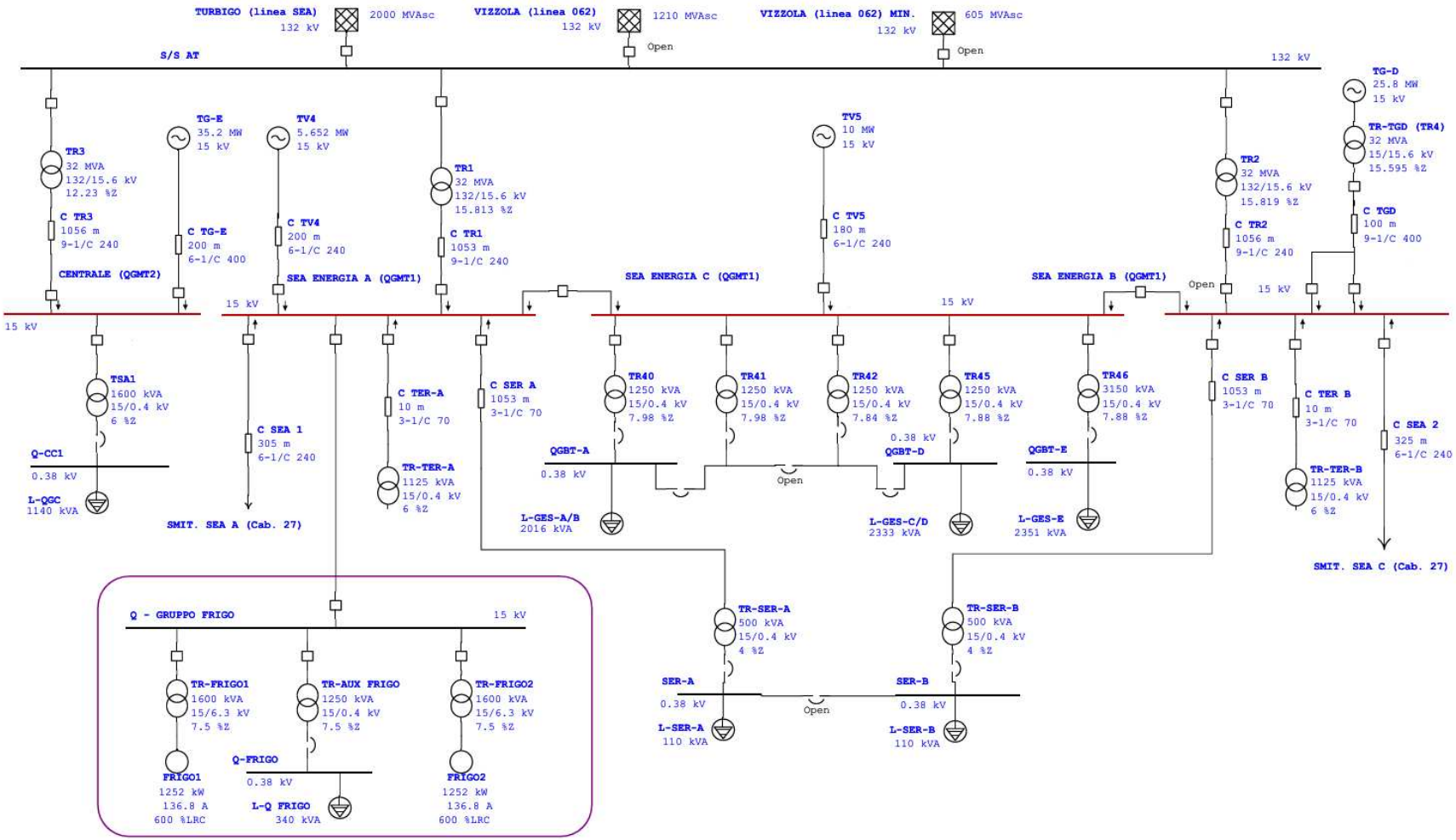

Figure 3.8: Etap Generation Model

Chapter 4

Fault Scenarios

4.1 Introduction

This chapter is structured as follows. First, the methodology adopted for the definition, computation, and interpretation of the Critical Clearing Time (CCT). Subsequently, the modifications introduced in the modelling of the 132 kV transmission interface are examined, with particular emphasis on the implementation of an equivalent overhead-line representation and its implications for electrical distance and fault severity.

4.2 Methodology for Transient Stability and Protection Evaluation

This section presents the methodology adopted to simulate electrical faults, evaluate generator stability, and determine protection performance within the electrical system of Milano Malpensa Airport. Because the ETAP Transient Stability module does not execute relay logic in real time, all protection operations are implemented manually using event sequencing. The objective is to combine manual clearing actions with analytical evaluation of relay thresholds to achieve a complete and rigorous stability assessment.

The methodology consists of four main phases:

1. determination of the Critical Clearing Time (CCT),
2. verification of protection selectivity under manual breaker clearing,
3. analytical evaluation of motor protections (49, 46, 48),

4. construction of a consistent event sequence for each simulation scenario.

4.2.1 Determination of the Critical Clearing Time (CCT)

The Critical Clearing Time represents the maximum duration for which a fault may remain on the system without causing loss of synchronism of the generators. Identifying the CCT is the first step in the analysis because protection clearing times must always be compared against the stability limit.

CCT Simulation Setup

To compute the CCT, a fault is applied at $t = 0$ at the relevant location in the network. Automatic relay logic is disabled, and instead a manual clearing action is added at a user-defined time (e.g. 80 ms, 100 ms, 120 ms). The simulation is repeated multiple times while progressively increasing the clearing time until instability occurs.

Stability Criteria

A clearing time is considered *stable* if generator rotor angles remain bounded, frequency and speed deviations settle to steady state, and terminal voltages recover to acceptable levels. A clearing time is *unstable* if rotor angle diverges continuously or if voltage collapses after fault clearing. The CCT is the largest clearing time for which the system remains stable.

4.2.2 Protection Behaviour Under Manual Clearing

Although real-time protection logic is not executed in ETAP, relay behaviour can still be evaluated by manually opening breakers at their known operating times and comparing the simulated electrical quantities with relay pickup thresholds.

Manual Breaker Operations

For each fault, the primary breaker is manually opened at its expected clearing time. To evaluate backup operation, the upstream breaker is opened at its backup delay (e.g. 300 ms).

Analytical Protection Evaluation

Protection behaviour is analysed using simulated current and voltage quantities. Over-current protection (50/51) is evaluated by comparing the fault current with pickup set-

tings and time-delay curves. Ground protection (51N) is assessed via residual or zero-sequence currents. Directional protection (67/67N) is evaluated using current direction and voltage sag characteristics. Although the relays do not operate automatically, the simulated quantities allow accurate determination of which device would trip first.

4.2.3 Evaluation of Motor Protections (49, 46, 48)

Motor protections in process-critical loads are not executed by ETAP during transient stability simulations. Their operation is inferred analytically. Thermal overload protection (49) is evaluated using RMS current and duration compared to thermal capacity. Phase-unbalance protection (46) is assessed through negative-sequence current. Stall protection (48) is examined using motor torque, slip and acceleration behaviour.

4.2.4 Event Sequencing in ETAP

A standardized event sequence is used for all simulations. For each scenario:

1. a fault is applied at $t = 0$,
2. the primary breaker is manually opened at its known clearing time,
3. the upstream breaker is opened only if backup performance is being evaluated,
4. the simulation is allowed to run until post-fault transients settle.

This event sequence supports CCT evaluation, protection-selectivity verification, and generator ride-through assessment under realistic clearing times. Although protection logic is not executed automatically, the combined manual-and-analytical methodology provides an accurate representation of real system behaviour.

4.3 Transmission Network Modeling for Fault Distance

Accurate assessment of fault severity requires realistic modeling of the 132 kV connection between Turbigo and the S/S AT bus. In this thesis, the transmission path was re-modeled using equivalent 132 kV overhead lines rather than MV cable sections to ensure correct impedance behavior. On the left side of the Figure 4.1 we see the original ETAP representation, in which the Turbigo source (2000 $\mathrm{MVA_{sc}}$, 132 kV) was connected

directly to the S/S AT busbar without an explicit line section. the right side of the Figure 4.1 illustrates the revised model, where two parallel overhead-line branches now constitute the transmission corridor between the HV bus and the S/S AT busbar.

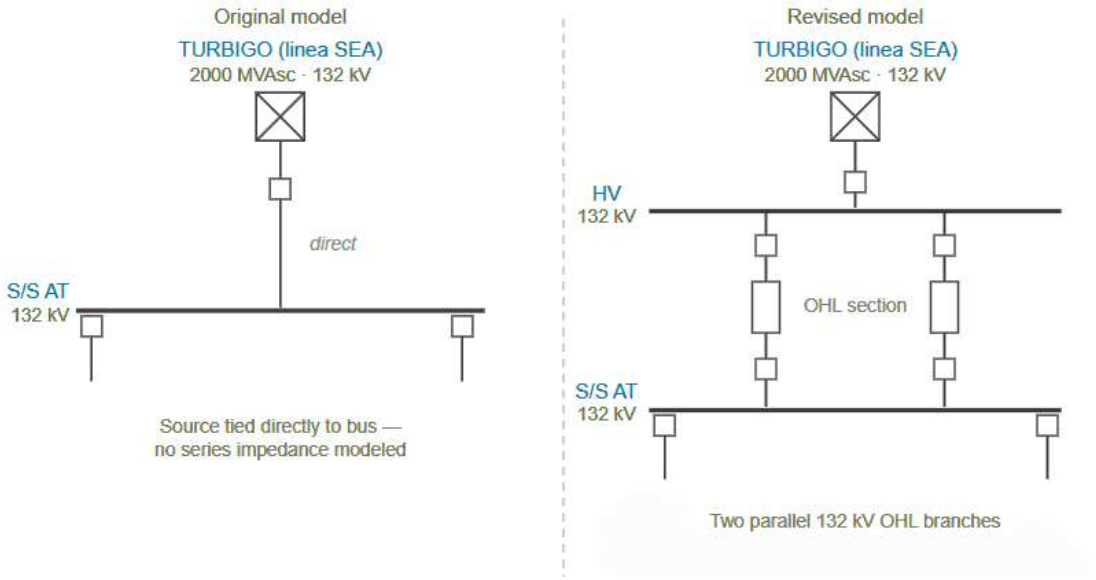

Figure 4.1: Revised model for transmission corridor

4.3.1 Transmission Line Parameters

The transmission corridor is represented using a 132 kV ACSR/AAAC overhead conductor (OXYGEN 337 mm^2), a configuration widely deployed in regional high-voltage networks due to its favorable thermal and mechanical characteristics. The positive-sequence electrical parameters adopted in this study are

$$R_1 \approx 0.090\ \Omega/\text{km}, \qquad X_1 \approx 0.380\ \Omega/\text{km}, \qquad B_1 \approx 2.7\ \mu\text{S/km},$$

leading to an X/R ratio of approximately 4.2. The conductor's ampacity lies in the 620–650 A range, and a fully transposed phase arrangement with a grounded overhead shield wire is assumed to reflect standard utility practice. These modeling choices ensure that the resulting positive-, negative-, and zero-sequence impedances are representative of realistic network behavior, thereby enabling credible analysis of SLG and other asymmetrical fault conditions [5].

4.3.2 Electrical Distance Modeling Strategy

To examine the sensitivity of system dynamics to the electrical location of a disturbance while maintaining a constant short-circuit strength of 2000 MVA at 132 kV, the line length was varied parametrically. Three distance regimes were defined:

- **Close-in faults** (1–5 km): emulate disturbances in the immediate vicinity of the source, characterised by large fault currents, pronounced voltage depressions, and significant electromechanical acceleration of synchronous machines.
- **Intermediate distances** (20–50 km): represent faults at moderate electrical distances, yielding moderate fault currents and voltage sags.
- **Remote faults** (80–100 km): simulate disturbances far from the infeed point, leading to reduced fault currents, shallower voltage sags, and inherently better damping of post-fault oscillations.

Adjusting only the series impedance in this manner allows the resulting fault current magnitude, voltage-sag depth, and rotor-angle response to evolve naturally with distance, without altering the underlying grid stiffness. This methodology is consistent with established transient stability assessment practices

4.4 Definition of Fault Types Considered

The study focuses on fault types that are most relevant for transient stability: single-line-to-ground (SLG) faults and three-phase (LLL) faults. These two classes capture the full spectrum of unbalanced and balanced disturbances likely to affect the system.

4.4.1 Single Line-to-Ground (SLG) Fault

An SLG fault occurs when one phase becomes short-circuited to ground and is the most common contingency in medium-voltage networks. It produces inherently unbalanced current and voltage profiles, substantial zero-sequence current flow, and voltage depression on unfaulted phases. Its severity is strongly influenced by system grounding conditions. SLG faults are central to protection and stability studies because, despite their moderate fault current magnitudes, they can induce significant electromechanical perturbations and frequently initiate protection operations.

4.4.2 Three-Phase (LLL) Fault

A three-phase bolted short circuit is the most severe and analytically fundamental disturbance. It produces the highest fault current levels, results in deep voltage collapse at the faulted bus, and excites only positive-sequence components due to its symmetry. This type of fault imposes the greatest electromechanical stress on synchronous generators and is therefore crucial for determining critical clearing times and assessing system stability margins. Together, SLG and LLL faults provide a comprehensive basis for evaluating system performance under both unbalanced and extreme balanced conditions.

4.5 Structure of the Fault Analysis

The investigation is organized into three scenarios, each reflecting a distinct category of disturbances affecting the airport electrical system.

- **Scenario A** considers a high-voltage disturbance at the 132 kV Turbigo interconnection (Linea SEA), representing conditions originating in the national transmission system.
- **Scenario B** examines an internal medium-voltage fault within the "Gruppo Frigo," the airport's principal chilled-water production plant.
- **Scenario C** addresses a fault on the 15 kV ring network beneath Cabina 27, a key distribution node supporting several airport subsystems.

These scenarios collectively encompass the primary sources of operational stress: external transmission level disturbances capable of propagating voltage depressions into the airport grid, internal medium voltage equipment faults involving large motor loads, and medium voltage ring topology events requiring sensitive and directional protection schemes.

4.6 Scenario A: HV Disturbance on the Turbigo (Linea SEA) Interconnection

Scenario A analyzes severe disturbances at the 132 kV Turbigo interface, such as lightning-induced faults on Linea SEA, transmission instability events, or equipment failures on

the Terna side. Given the strong electrical coupling between the airport and the national transmission system, such events can induce significant voltage excursions and electromechanical disturbances within the airport grid.

4.6.1 Protection Coordination Requirements

At the 132 kV point of interconnection, the airport network operated by SEA is directly coupled to the Italian Transmission System (RTN) managed by Terna, and the protection schemes on both sides must therefore operate in a selective and coordinated manner. When a fault occurs inside the airport network, SEA's protection relays are required to clear the disturbance before any intervention by Terna, ensuring that internal faults do not propagate upstream and preventing unnecessary disconnection of the airport from the national grid. Conversely, faults originating on the RTN must be cleared primarily by Terna's high-voltage protection systems, with SEA's relays providing only a coordinated backup function. In accordance with operational practice, this backup clearing is modelled with a maximum interruption time of approximately 300 ms.

To accurately represent this protection philosophy, the ETAP model incorporates SEA's realistic 132 kV relay settings and breaker clearing times, including distance, instantaneous, time-overcurrent, directional, and voltage-restrained elements (ANSI 21, 50/51, 67, 51V), together with the associated teleprotection logic that enables rapid tripping of both line terminals when required. Terna's protection behaviour is represented through its multi-zone distance protection, transfer-trip arrangements, intentional time delays, and the relevant instrument transformer ratios. This detailed modelling ensures that the simulated clearing sequences and their effects on rotor-angle stability, frequency deviation, and critical clearing times are reproduced with high fidelity.

4.7 Scenario B: Internal MV Fault in the "Gruppo Frigo"

Scenario B addresses a medium-voltage fault within the Gruppo Frigo, the airport's most energy-intensive facility and a major source of dynamic load behavior. The plant supplies large induction machines whose electromagnetic and mechanical characteristics significantly influence system stability during disturbances.

4.7.1 Analytical Objectives

The simulation focuses on characterizing feeder behavior under high-magnitude MV faults, evaluating protection selectivity between incomers, MCCs, and motor starters, and assessing the operation of thermal, unbalance, and overcurrent protection elements (49, 46, 50/51, 51N). The interaction between fault-induced torque disturbances, motor stalling tendencies, and generator electromechanical stability is closely examined. The scenario incorporates detailed information on the induction machines used in the gruppo frigo and their capabilities. Any load-shedding strategies or safety interlocks associated with the compressors or auxiliary systems are also explicitly included to ensure a realistic representation of plant behavior during faults.

4.8 Scenario C: 15 kV Ring (Anello) Fault Under Cabina 27

Scenario C investigates the behaviour of the medium-voltage ring network ("anello") located downstream of Cabina 27. This portion of the distribution system is characterized by looped feeder topology, the presence of directional protection elements, and the integration of the airport's photovoltaic (PV) generation system. Because of this configuration, faults occurring in any segment of the ring can lead to complex interactions between directional relay logic, feeder selectivity, and the inverter-based generation attached to the network.

4.8.1 Analytical Objectives

The objective of Scenario C is to analyse how a fault on the 15 kV ring affects:

- the **Operation of directional overcurrent protection** (67/67N) in the looped network,
- the **Fault-clearing times and selectivity** among ring feeders,
- the **Post-fault voltage and frequency recovery** at nearby buses,
- the **Dynamic response of synchronous generators** (TG units and TV units),
- the **PV system behaviour**, both *connected* and *disconnected*,

This scenario, therefore, combines conventional generator electromechanical stability assessment with the behaviour of inverter-based resources during network disturbances.

4.8.2 PV System Considerations During MV Ring Faults

The impact of the PV plant on system dynamics is evaluated under two operating modes:

1. **PV Connected**: the inverter contributes limited fault current and interacts with voltage and frequency ride-through thresholds.
2. **PV Disconnected**: the network is supplied only by synchronous generation, providing a baseline to assess the incremental severity introduced by the PV system.

During an SLG or LLL fault on the anello, the PV inverter experiences:

- a **Temporary voltage sag**, whose magnitude depends on electrical distance from the fault,
- a possible **Frequency deviation** following generator power oscillations,

The inverter may either *ride through* the disturbance (remaining synchronized and injecting active/reactive current) or *disconnect* if voltage or frequency thresholds are violated for longer than permitted by its internal protection delays. This behaviour has a direct effect on the post-fault power balance and can influence generator rotor-angle trajectories and voltage recovery. This scenario therefore provides a comprehensive view of the dynamic interactions between traditional synchronous generation, inverter-based resources, and MV ring protection during realistic operating disturbances.

Chapter 5

Transient Stability, Protection Behaviour, and Resiliency Assessment

This chapter presents a comprehensive and integrated analysis of the dynamic behaviour, protection performance, and operational resiliency of the electrical system of Milano Malpensa Airport under a selection of representative high-voltage (HV) and medium-voltage (MV) disturbances. The work builds directly upon the methodological framework established in the previous chapter, which introduced the Critical Clearing Time (CCT), the manual event-sequencing approach used in ETAP transient stability simulations, the analytical protection-evaluation method, and the modelling of transmission-line electrical distances. The present chapter operationalises these concepts by applying them to three realistic disturbance scenarios and by deriving engineering conclusions regarding stability margins, protection adequacy, and the structural resiliency of the airport's electrical system.

The chapter is organised into three principal components. First, the transient stability results are presented for three fault scenarios: an external HV fault at the Turbigo (Linea SEA) interconnection, an internal MV radial fault involving the Gruppo Frigo subsystem, and a disturbance within the 15 kV ring network beneath Cabina 27, including the contribution of the 10 MW photovoltaic (PV) plant. Second, an analytical protection assessment is performed using both IEC 60909 short-circuit currents and the voltage/current waveforms obtained from transient simulations. Third, the overall re-

siliency of the network is examined, including identification of single points of failure (SPOFs) and a technical discussion on the feasibility of islanded operation.

5.1 Methodological Integration with Previous Thesis Sections

All analyses presented here adhere strictly to the modelling framework developed earlier in the thesis. The transient simulations employ the event sequencing strategy described previously in Chapter 4 , in which faults are initiated at $t = 0\,\mathrm{s}$ and breaker clearing is executed manually at known protection operating times. As established previously, a total clearing time of 60 ms is applied for HV faults at the 132 kV interface reflecting the combined operation of distance and pilot protection while MV disturbances are cleared after 80 ms, consisting of a 20 ms relay decision time followed by a 60 ms mechanical opening time. Backup clearing at approximately 300 ms is introduced only when explicitly required for selectivity studies.

Protection behaviour is evaluated analytically using simulated current magnitudes, voltage depressions, phase-angle relationships, and zero-sequence ($3I_0$) quantities. This procedure follows the protection methodology developed earlier for ANSI functions 50/51, 51N, 67/67N, 49, 46, and 48. IEC 60909 short-circuit calculations supplement this analysis by providing the fault-current magnitudes and source contributions necessary for validating pickup thresholds.

The fault types simulated in this chapter correspond exactly to those defined previously: the single-line-to-ground (SLG) fault, which produces unbalanced voltage and current conditions and is the most common MV contingency, and the three-phase (LLL) fault, which represents the most severe balanced disturbance for transient stability assessment. The modelling of the 132 kV corridor using overhead-line parameters ensures that Scenario A reflects realistic electromagnetic behaviour across a range of electrical distances.

To frame the analytical structure of this chapter, Table 5.1 summarises the objectives, guiding questions, and required fault coverage associated with transient stability, protection pickup, and resiliency analysis.

This structure ensures that the three analytical components remain consistent with one another and with the modeling philosophy implemented.

Table 5.1: Overview of study objectives and fault-coverage requirements.

Study Type	**Objective**	**Engineering Question**	**Fault Coverage Needed**
Transient Stability (A/B/C)	Electromechanical stability; voltage and frequency dynamics	Do generators remain synchronised? Do voltages recover after fault clearing?	Worst-case and structurally representative locations
Protection Pickup (IEC 60909)	Sensitivity and selectivity of protective devices	Will relays detect the fault? Is the clearing time realistic?	Representative HV and MV locations
Resiliency Assessment	Architectural robustness	Are there SPOFs? How does topology influence continuity?	Critical MV buses and supply paths

5.2 Scenario A: High-Voltage Disturbance on the Turbigo (Linea SEA) Interconnection

5.2.1 Context and Objective

Scenario A evaluates a severe disturbance at the 132 kV interconnection with the SEA Energia/Terna grid. As discussed in Chapter 4, transmission-level faults induce deep voltage depressions and transient electromagnetic torque imbalance, making them the most demanding electromechanical events for synchronous generators. The aim of Scenario A is to verify whether TG–E and TV5 remain stable under such disturbances, whether voltage and frequency recover adequately, and whether the adopted 60 ms clearing time lies comfortably below the critical clearing boundary.

5.2.2 Fault Modelling and Clearing Time

The analysis of Scenario A follows directly from the methodological framework outlined before, where both the Critical Clearing Time (CCT) determination and the electrical-distance modelling strategy were established. Accordingly, the 132 kV disturbance at the S/S AT bus was studied through a combination of:

1. **CCT sweep simulations**, in which the fault-clearing time is progressively increased beyond the nominal value (60 ms) until instability is observed, and

2. **fault-distance sensitivity**, in which the effective electrical distance between

Malpensa and the Turbigo substation are varied by adjusting the length of the 132 kV overhead-line model presented in the section on Transmission Network Modeling for Fault.

Two disturbance types were imposed:

- A bolted three-phase short circuit (LLL), representing the most severe balanced disturbance for which the CCT is typically defined, and
- A single-line-to-ground (SLG) fault, which is the most common asymmetrical disturbance in transmission systems.

For the base comparison with protection requirements, both faults were cleared at 60 ms, consistent with SEA/Terna high-voltage protection coordination. Additional clearing times (80 ms, 100 ms, 120 ms) were considered in the CCT sweep to identify the maximum clearing time that preserves synchronism.

Likewise, the overhead-line length was varied between 1–5 km (close-in fault), and 80–100 km (remote fault), following the electrical- distance methodology introduced previously. This allowed the analysis to capture the natural reduction in fault current and voltage sag severity as the fault location becomes electrically more distant.

5.2.3 CCT sweep results

The CCT sweep was carried out for the close-in three-phase fault at the 132kV interface, extending well beyond the nominal protection operating time. The system remained transiently stable for clearing times up to 1s, with bounded and decaying rotor-angle oscillations. No loss of synchronism was observed within the investigated range. Consequently, the Critical Clearing Time exceeds the maximum clearing time tested, confirming that the adopted high voltage protection scheme operates with a very wide stability margin (defined as unbounded rotor-angle divergence).

This result confirms that:

- The HV protection scheme clears faults well below the CCT;
- The generation system possesses an adequate transient-stability reserve;
- External HV faults do not represent a limiting condition for grid-connected operation.

Table 5.2: Clearing-time sweep results for a close-in three-phase fault at the 132 kV interface (Scenario A).

Clearing Time	**Minimum Voltage at Generator Terminals**	**Rotor-Angle Behaviour**	**Post-Fault Dynamic Response**	**Stability Outcome**
60 ms (actual protection time)	$V \approx 0$ pu during fault interval	Bounded rotor-angle excursion	Well-damped oscillations settling within $\sim$10 s	Stable
100 ms	$V \approx 0$ pu during fault interval	Larger but bounded oscillations	Reduced damping with eventual settling	Stable
300 ms	$V \approx 0$ pu during fault interval	Pronounced but bounded oscillations	Longer settling time with preserved synchronism	Stable
1 s	$V \approx 0$ pu during fault interval	Large rotor-angle deviation without divergence	Slowly damped oscillations; no pole slipping observed	Stable

5.2.4 Electromechanical Response

The bolted three-phase (LLL) fault produced a deep and abrupt voltage collapse at the generator terminals, as shown in Figure 5.1, leading to a severe electromechanical disturbance. This voltage collapse is expected, since a three-phase short circuit effectively eliminates the positive-sequence network at the fault location, thereby removing the principal source of electromagnetic synchronising torque. As a consequence, the synchronous generators experienced a rapid acceleration, reflected in the rotor-angle excursions shown in Figure 5.2 and the corresponding speed deviations reported in Figure 5.3.

Despite the severity of the disturbance, the generators remained synchronised. Following fault clearing, the rotor-angle trajectories of TG–E and TV5 exhibited well-damped oscillations, indicating adequate system damping across all electrical distances analysed. The associated frequency response, illustrated in Figure 5.4, shows a transient frequency deviation that remains within acceptable limits and recovers smoothly after clearing. For electrically more remote faults, the voltage sag at the generator terminals was less pronounced, leading to proportionally smaller rotor-angle and frequency deviations, in accordance with the increased positive-sequence impedance of the 132 kV corridor.

In contrast, the single-line-to-ground (SLG) fault produced markedly milder electromechanical effects, as evidenced by the rotor-angle behaviour shown in Figure 5.5. In this case, only one phase voltage collapses, while a substantial positive-sequence voltage component is retained throughout the fault interval, as illustrated in Figure 5.6. As discussed in Section **??**, the positive-sequence network governs the synchronising torque of synchronous machines; therefore, the partial retention of positive-sequence voltage explains the limited rotor-angle excursions observed for SLG faults. Consistently, both system frequency and generator terminal voltage, shown in Figure 5.7, returned to nominal values within a short post-fault interval, confirming the inherently lower severity of SLG disturbances with respect to three-phase faults.

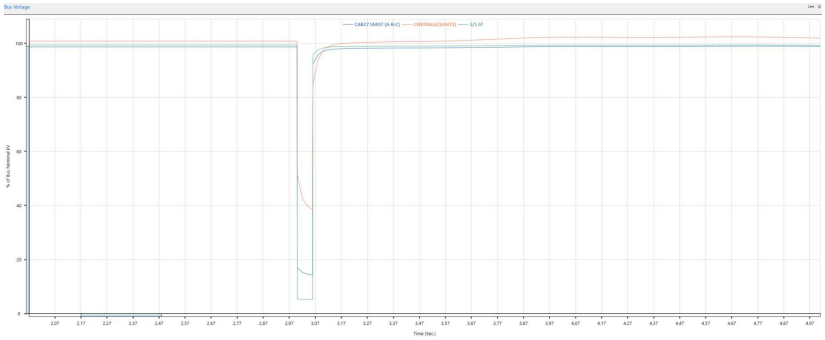

Figure 5.1: Voltage Sag for LLL close Fault

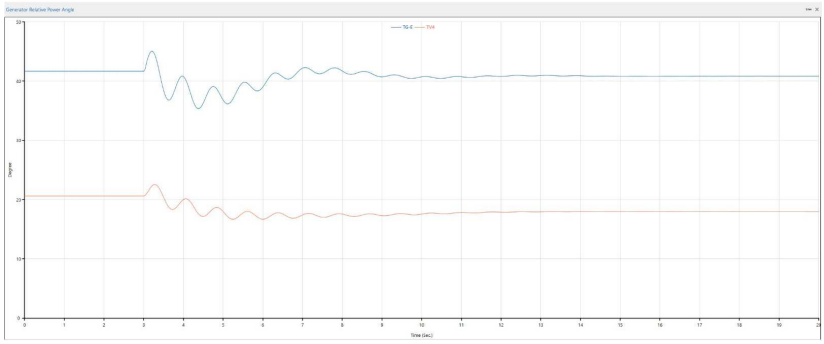

Figure 5.2: Power Angle variation For LLL close Fault

5.2.5 Scenario A Conclusion

Scenario A demonstrates that the Malpensa cogeneration plant possesses substantial transient-stability margins under transmission-level disturbances. The 60 ms clearing time adopted by SEA/Terna lies well below the CCT obtained from the sweep simulations, ensuring rotor angle stability even under close in, three-phase faults. Furthermore, the electrical-distance sensitivity confirmed that fault severity decreases monotonically

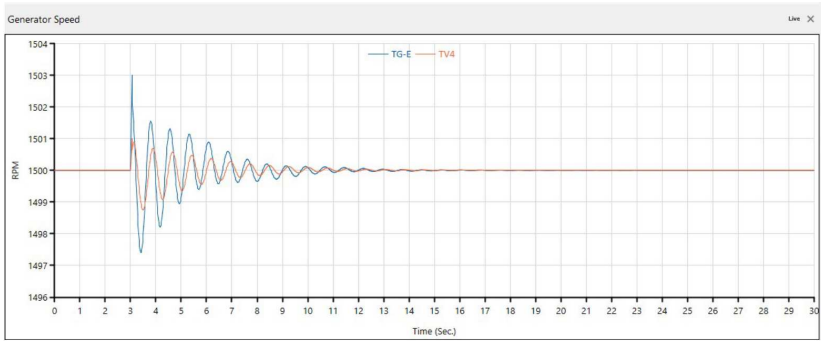

Figure 5.3: Generator Speed Variation for LLL close Fault

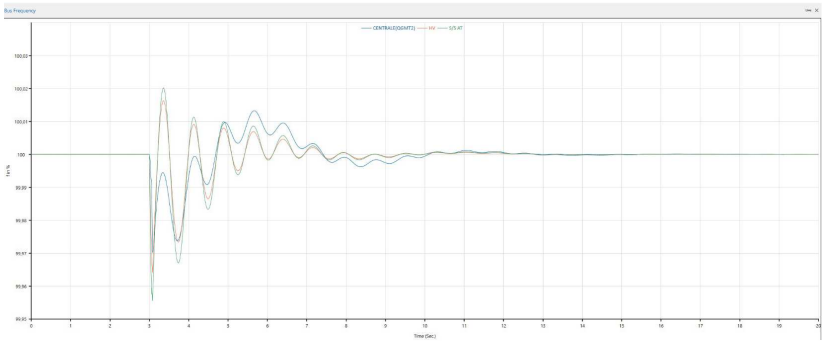

Figure 5.4: Frequency Response for LLL close Fault

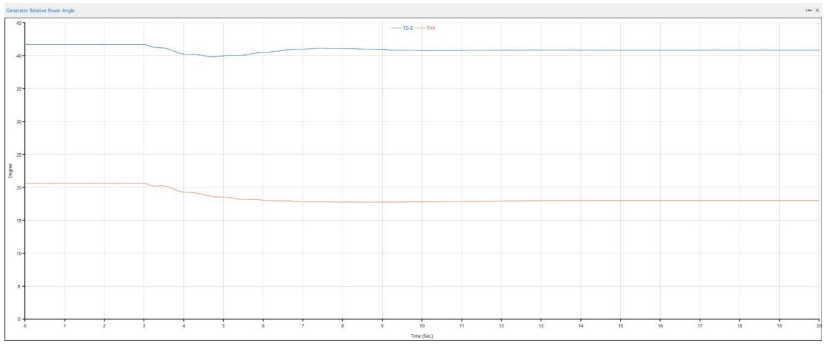

Figure 5.5: Power Angle variation for SLG close Fault

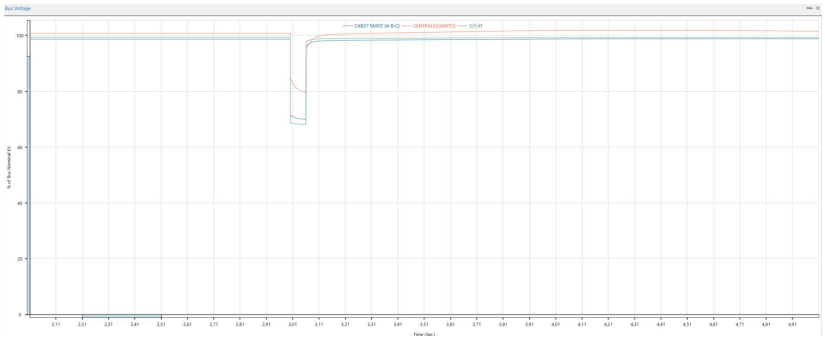

Figure 5.6: Voltage Sag for SLG close Fault

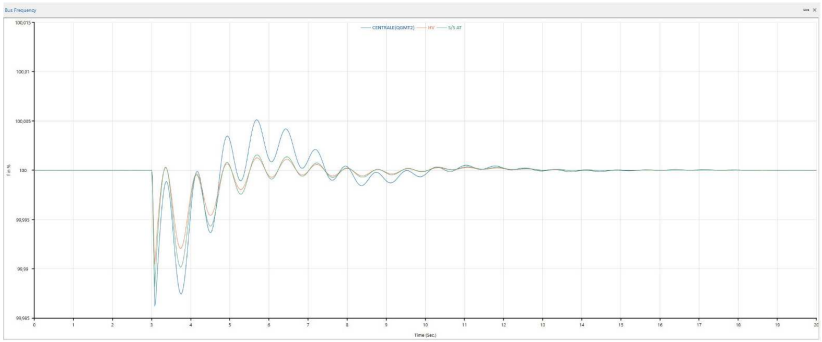

Figure 5.7: Frequency Response for SLG close Fault

with increasing line impedance, as expected from the theoretical behaviour of the positive-sequence network. SLG faults, due to their partial retention of positive-sequence voltage, were consistently less severe than LLL disturbances.

Overall, Despite the severity of the HV fault and the deep voltage depression, all generator protection elements remain inactive Scenario A confirms that generator ride-through capability is robust across the full range of fault distances and clearing times relevant to the 132 kV interface.

5.3 Scenario B: Internal MV Radial Fault in the *Gruppo Frigo*

5.3.1 Background and Motivation

Scenario B examines an internal disturbance in the MV radial feeder powering the *Gruppo Frigo*, a major chilled-water production facility consisting of two large induction-motor-driven compressors (FRIGO1 and FRIGO2) and several auxiliary loads. As established previously, the entire subsystem is fed from a single MV bus (Q–GRUPPO FRIGO), making it a clear Single Point of Failure (SPOF). The objective of Scenario B is to evaluate generator stability under MV disturbances, protection selectivity between bus and feeder faults, and the general resiliency of the radial topology.

5.3.2 Disturbance Definition and Clearing Time

The following disturbances were simulated with an 80 ms clearing time:

- Three-phase fault at Q–GRUPPO FRIGO (bus fault),
- Three-phase faults at the FRIGO1 and FRIGO2 feeders,
- SLG faults at the same locations,
- Representative LV auxiliary faults.

5.3.3 Electromechanical Response

The bus-level three-phase (LLL) fault at the Q–GRUPPO FRIGO medium-voltage bus caused the immediate disconnection of the refrigeration subsystem, thereby activating the single point of failure inherent to the radial supply architecture. This outcome confirms that the primary vulnerability identified in Scenario B is architectural in nature. Nevertheless, the on-site synchronous generation units remained dynamically stable throughout the disturbance, indicating that the system possesses adequate electromechanical stability margins for internal MV faults.

From a voltage perspective, the disturbance is strongly localized. The upstream high-voltage interface experiences only a moderate voltage depression, reflecting the stiffness of the 132 kV network and its ability to support the system during severe downstream disturbances. A more pronounced voltage sag is observed at the MV radial bus feeding the refrigeration plant, while the most severe voltage collapse occurs at

the Q–GRUPPO FRIGO bus itself, where the voltage drops to zero due to the bolted three-phase fault.

Following fault clearance, the Q–GRUPPO FRIGO bus remains de-energized as part of the protective isolation of the refrigeration subsystem; therefore, voltage recovery is not observed at the faulted bus. In contrast, the upstream MV radial bus and the high-voltage interface recover rapidly after fault clearing, confirming that the voltage disturbance does not propagate beyond the immediate vicinity of the faulted radial segment (Figure 5.11).

A closer examination of the generator responses highlights a non-uniform contribution to the fault. In particular, generator TV4, which is electrically closer to the Q–GRUPPO FRIGO bus, supplies the dominant share of the short-circuit current during the fault. This behaviour is clearly visible in the generator current waveforms shown in Figure 5.10. The higher current contribution of TV4 is consistent with classical short-circuit theory, according to which fault currents are preferentially supplied by sources with the lowest electrical impedance to the fault location.

As a direct consequence of this higher electrical stress, generator TV4 exhibits larger yet still well-damped electromechanical oscillations. This behaviour is reflected in the rotor-angle response illustrated in Figure 5.8 and in the corresponding speed variations shown in Figure 5.9. In contrast, the generator that is electrically farther from the fault location experiences significantly smaller deviations in angle, speed, and electrical power, consistent with its reduced participation in the fault current.

The system frequency response further confirms the benign dynamic behaviour of the generation units. As illustrated in Figure 5.12, the frequency deviation remains limited during the disturbance and returns smoothly to nominal values after fault clearance, with no indication of instability or activation of emergency frequency control actions.

For feeder-level faults within the Gruppo Frigo subsystem, protection selectivity is successfully achieved: only the faulted compressor feeder is isolated, while unaffected feeders remain in service. Minor variations in voltage sag observed between the FRIGO1 and FRIGO2 cases can be attributed to normal cable-impedance asymmetries. Single-line-to-ground and low-voltage auxiliary faults produce significantly milder electromechanical effects, characterized by shallow voltage depressions, rapid recovery, and negligible impact on generator dynamics.

Overall, Scenario B demonstrates that internal MV faults predominantly stress the generator that is electrically closest to the disturbance, while the strong upstream grid effectively limits voltage and frequency excursions. The observed behaviour confirms

that the dominant limitation associated with the Gruppo Frigo supply lies in its radial topology rather than in any deficiency of the generation system's transient-stability performance.

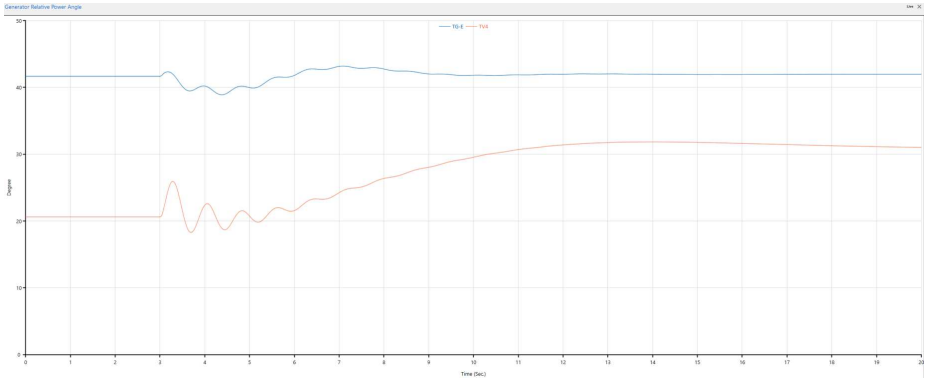

Figure 5.8: Power angle for LLL fault at Gruppo Frigo main bus

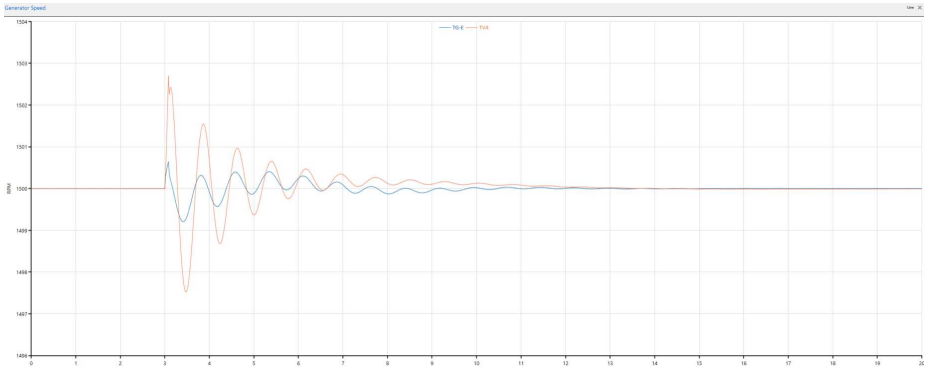

Figure 5.9: Generators Speed for LLL FAULT at Gruppo Frigo main bus

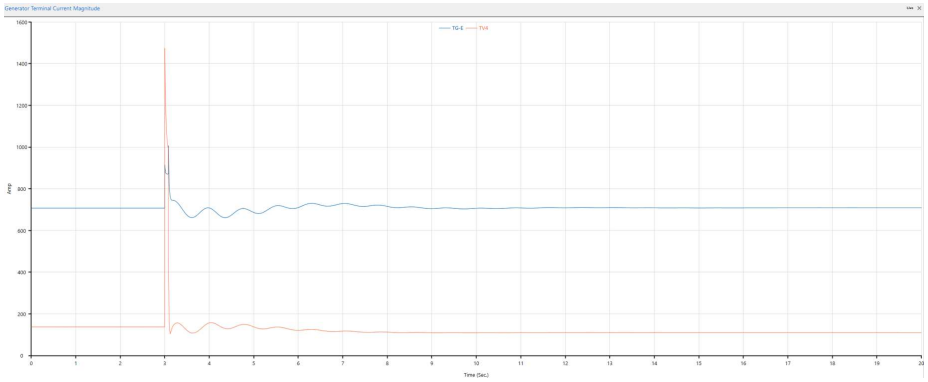

Figure 5.10: Current seen by Generators for LLL fault at Gruppo Frigo main bus

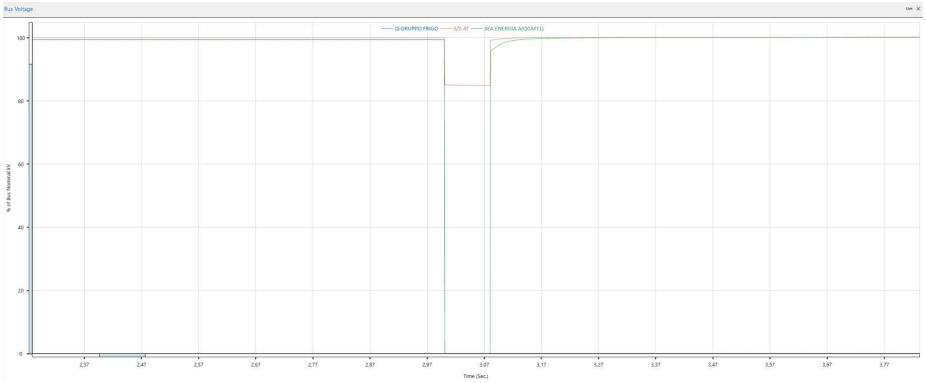

Figure 5.11: Bus voltage sag for LLL fault at Gruppo Frigo main bus

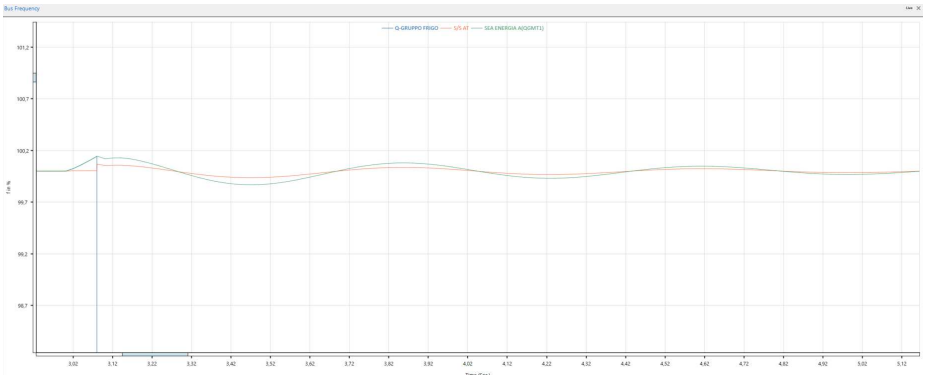

Figure 5.12: Bus frequency response for LLL fault at Gruppo Frigo main bus

5.3.4 Analytical Motor-Protection Evaluation

Given the absence of dynamic induction-machine models in the ETAP student license, motor-protection functions (49, 46, 48) were evaluated analytically. The torque–voltage relation $T \propto V^2$ implies that the voltage depressions observed never approached levels associated with centrifugal-compressor stalling. Accordingly, no stall, thermal, or unbalance protection operation is expected for the short, well-cleared faults in this scenario.

5.3.5 Scenario B Conclusion

Scenario B demonstrates that while generator stability is consistently preserved for internal MV faults, the radial structure of the *Gruppo Frigo* supply path constitutes a significant resiliency limitation. The Q–GRUPPO FRIGO bus is conclusively identified as a Single Point of Failure.

5.4 Scenario C: 15 kV Ring Network Fault Under Cabina 27 with PV Integration

5.4.1 Motivation and System Characteristics

Scenario C concerns a disturbance within the looped 15 kV ring feeding a range of airport subsystems. The looped topology requires directional protection, and the proximity of a 10 MW PV plant adds considerations related to inverter-based voltage support, fault-current limitations, and frequency dynamics. This scenario therefore examines both the electromechanical response and protection behaviour under ring-network faults.

5.4.2 Disturbances Simulated

At Cabina 27, the following disturbances were applied:

- A three-phase fault,
- A single-line-to-ground fault,
- Each simulated with PV connected (ON) and disconnected (OFF).

An 80 ms clearing time was maintained for all cases.

5.4.3 Electromechanical Response

When the photovoltaic (PV) plant is connected to the MV ring network, the voltage response during faults exhibits improved resilience. In particular, voltage depressions at the MV buses are shallower, as shown in Figure 5.13. This behaviour is attributable to the local active-power injection provided by the PV plant, which supports the voltage during and immediately after fault clearance. In contrast, the voltage at the high-voltage 132 kV bus remains nearly unaffected, exhibiting only negligible variations , owing to its electrical remoteness from the faulted MV network and the high short-circuit strength of the transmission system.

The frequency response with the PV plant connected shows a slightly larger initial deviation following the fault. This behaviour is expected, since the PV plant operates as a grid-following inverter and does not contribute rotational inertia or synchronising torque. Nevertheless, the frequency deviation remains within acceptable limits and recovers smoothly after fault clearing, while both synchronous generators remain stable.

When the PV plant is disconnected, the system response changes subtly. The voltage sag at the MV buses becomes more pronounced shown in Figure 5.14. However, the high-voltage bus again experiences negligible voltage disturbance, confirming that upstream transmission nodes are largely decoupled from MV level fault dynamics. The frequency deviation in the PV OFF case is slightly less pronounced,reflecting the unchanged inertial contribution of the synchronous generators and the absence of inertial-less PV interaction.

Overall, the comparison between PV ON and PV OFF conditions demonstrates that the presence of the PV plant enhances local voltage performance without adversely affecting generator stability. In all simulated disturbances, rotor-angle trajectories remain bounded, voltage recovers at all non-faulted buses, and frequency deviations decay without the activation of additional control or protection mechanisms, confirming that the system operates with ample transient-stability margins under both operating conditions.

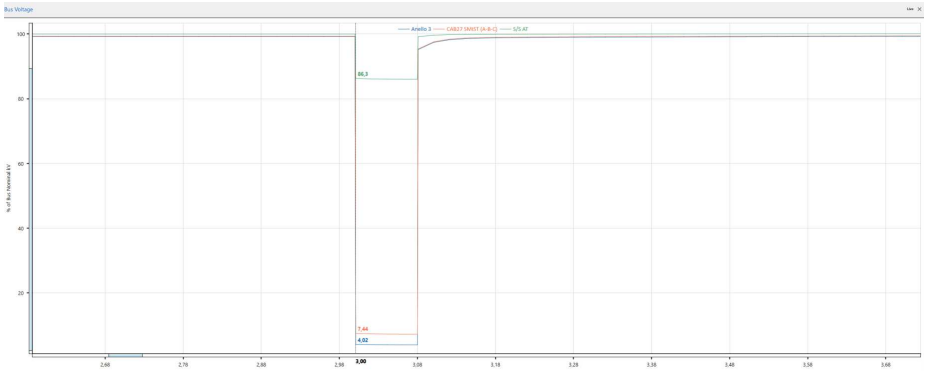

Figure 5.13: Voltage response after LLL fault with PV connected in MV

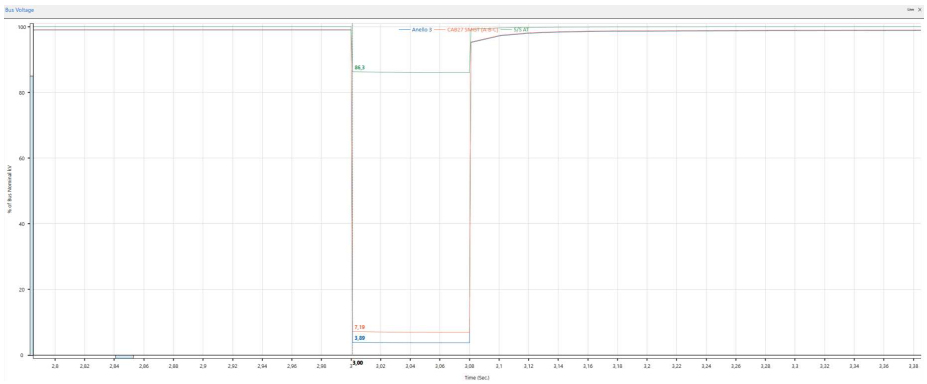

Figure 5.14: Voltage response after LLL fault with PV disconnected in MV

5.4.4 Scenario C Conclusion

Scenario C demonstrates that while PV integration noticeably improves MV voltage resilience, generator rotor-angle stability is essentially unaffected. The looped topology proved robust, and directional discrimination operated effectively in all studied cases.

5.5 Analytical Protection Evaluation for all scenarios

The analytical protection evaluation combines the simulated electrical quantities from transient analyses with IEC 60909 short-circuit results. This approach enables determination of pickup, directionality, and selectivity of key protection elements, despite the absence of real-time protection emulation in ETAP.

5.5.1 Phase Overcurrent (50/51)

Short-circuit calculations revealed that MV three-phase faults at Q–GRUPPO FRIGO and Cabina 27 produced fault currents in the range of 15–16 kA, while SLG faults produced approximately 8–9 kA. These magnitudes exceed typical pickup thresholds for 50/51 protections by a wide margin (1.5–2.5 kA), ensuring reliable phase-fault detection for all modeled contingencies. HV LLL faults at S/S AT produced approximately 6 kA at 132 kV, also well above pickup requirements.

5.5.2 Ground Overcurrent (51N)

Residual-current behaviour was evaluated using the simulated zero-sequence quantity $3I_0$. SLG faults produced substantial residual current dominated by the grounded synchronous generators. The PV inverter, being grid-following and current-limited, contributed negligible zero-sequence current and therefore does not impair ground-fault sensitivity. All 51N elements are expected to operate correctly for SLG disturbances.

5.5.3 Directional Protection (67/67N)

Directional behaviour was evaluated using positive-sequence current angles, active-power flow, and voltage-phase relationships. In all ring-network cases, the feeder supplying the fault exhibited a clear forward direction. The presence of the PV plant did not distort directional characteristics sufficiently to interfere with correct relay operation.

This confirms that directional overcurrent schemes remain effective under all modeled disturbances.

5.5.4 Protection Logic Flow Interpretation

The simulated behaviours across Scenarios B and C conform to the conceptual protection-logic sequence developed earlier in the thesis:

1. a fault causes current magnitude to exceed pickup;
2. a directional check is performed;
3. if the direction is forward, the feeder breaker trips;
4. if reverse or ambiguous, the local operation is blocked and upstream clearing occurs.

This behaviour was consistently observed in all transient analyses and is further supported by the short-circuit results.

Table 5.3: Protection Logic evaluation for Scenario A

ANSI Function	**Relevant Quantity**	**Analytical Observation**	**Expected Operation**
50/51	Phase current magnitude	LLL $\approx 6\,\text{kA}$ at S/S AT; typical pickup 1–2 kA.	Pickup certain; fast tripping by HV protection.
51N	Residual current ($3I_0$)	SLG produces measurable zero-sequence current through grounded transformers.	Sensitive SLG pickup; SEA acts as backup, Terna clears fault.
67	Direction of I_1 vs. V_1	Clear forward direction into S/S AT; fault sourced predominantly from the transmission grid.	External fault confirmed; SEA blocks directional elements, Terna clears.
67N	Direction of $3I_0$	Zero-sequence current direction indicates an external ground fault.	Reverse direction; 67N elements intentionally blocked.
46	Negative-sequence current	SLG causes moderate I_2; duration too short to impact machine heating limits.	No tripping; unbalance acceptable.
49	Thermal equivalent (I^2t)	Fault clearing $< 0.1\,\text{s}$ produces negligible thermal stress.	No thermal operation.
48	Motor stall	Not applicable at the HV interface.	Not applicable.

Table 5.4: Generator protection evaluation for Scenario A (HV fault at S/S AT, 132 kV).

Protection	**Relevant Quantity**	**Analytical Observation**	**Expected Response**
87G/87T (Differential)	Internal generator / GSU zone	No internal generator or step-up transformer faults were simulated.	No trip.
51V / 27 (Undervoltage / V–restrained OC)	Terminal voltage V_t	LLL fault produces $V_t \approx 0$ pu for ~ 60 ms; duration below UV/51V trip thresholds.	No trip (generator ride-through).
78 (Out-of-step)	Rotor-angle trajectory $\delta(t)$	Large initial acceleration followed by bounded, well-damped oscillations; no pole slipping.	No loss of synchronism; no trip.
81U/81O (Under/Over-frequency)	Frequency deviation Δf	Frequency remains within ± 0.5 Hz due to strong external grid support.	No frequency protection operation.
40 (Loss of excitation)	Reactive-power / field behaviour	Reactive power remains positive; no leading VArs or loss-of-field signature observed.	No LOE trip.
24 (Overexcitation)	V/f ratio	Voltage depression during fault reduces magnetic flux; no overfluxing condition.	No overexcitation trip.
46 (Negative sequence)	Negative-sequence current I_2	SLG faults generate moderate I_2 for short duration; within permissible limits.	No unbalance tripping.
49 (Thermal)	Thermal equivalent I^2t	Fault clearing < 0.1 s results in negligible thermal stress.	No thermal operation.
Feeder isolation	Generator incomer breaker status	HV-side protection clears the fault; generator feeders remain closed.	Generators remain online.

Table 5.5: Protection logic evaluation for Scenario B

ANSI Function	**Relevant Quantity**	**Analytical Observation**	**Expected Operation**
50/51	Phase current magnitude	LLL at Q–GRUPPO FRIGO $\approx 16\,\text{kA}$; feeder pickup typically 1.5–2.5 kA.	Immediate pickup; selective isolation of the affected bus or feeder.
51N	Residual current ($3I_0$)	SLG produces $\approx 8\,\text{kA}$ zero-sequence current dominated by grounded synchronous generators.	Fast and sensitive SLG pickup; correct for both bus- and feeder-level faults.
67	Power-flow direction and I_1 angle	Strong forward current during faults on FRIGO1 and FRIGO2 feeders; clear directional signature.	Trips only the faulted feeder; maintains selectivity.
67N	Residual-current direction ($3I_0$)	Zero-sequence direction remains clearly forward for SLG faults on either feeder.	Reliable SLG directional discrimination.
46	Negative-sequence current	LLL faults produce negligible I_2; SLG faults produce moderate unbalance for $< 80\,\text{ms}$.	No unbalance tripping; negative-sequence within allowable short-duration limits.
49	Thermal model (I^2t)	Fault duration $< 0.1\,\text{s}$; no significant thermal accumulation in feeders or motors.	No thermal element operation.
48	Motor stall (for FRIGO compressors)	V_{min} remained $> 0.80\,\text{pu}$ for $< 100\,\text{ms}$; torque $T \propto V^2$ well above stall threshold.	No motor stall; compressors ride through the disturbance.

Table 5.6: Generator protection logic evaluation for Scenario B

Protection	**Relevant Quantity**	**Analytical Observation**	**Expected Response**
87G/87T (Differential)	Internal generator/GSU zone	No internal electrical disturbance or differential fault simulated.	No trip.
51V / 27 (Undervoltage / V–restrained OC)	Terminal voltage V_t	MV faults produced only mild sags; V_t remained above 0.7 pu.	No trip (voltage well above UV thresholds).
78 (Out-of-step)	Rotor-angle trajectory $\delta(t)$	Rotor-angle deviations were very small; no divergence or slip cycles.	No loss of synchronism; no trip.
81U/81O (Under/Over-frequency)	Frequency deviation Δf	Frequency deviation remained < 0.2 Hz during all MV disturbances.	No frequency protection operation.
40 (Loss of excitation)	Reactive-power / field indicators	No leading reactive-power behaviour or field-weakening signatures observed.	No LOE trip.
24 (Overexcitation)	V/f ratio	Flux and V/f remained within normal limits; no overvoltage conditions.	No overexcitation trip.
46 (Negative sequence)	Negative-sequence current I_2	SLG faults produced minor I_2 for less than 80 ms.	No tripping; unbalance within permissible duration.
49 (Thermal)	Thermal equivalent I^2t	Clearing time ≤ 80 ms resulted in negligible heating.	No thermal protection operation.
Feeder isolation	Feeder breaker status	Only Gruppo Frigo feeders opened during faults; generator feeders remained energised.	Generators remain online.

Table 5.7: Protection logic evaluation for Scenario C

ANSI Function	**Relevant Quantity**	**Analytical Observation**	**Expected Behaviour**
50/51 (Phase Overcurrent)	Fault current magnitude	LLL $\approx 15.8\,\text{kA}$; SLG $\approx 8.2\,\text{kA}$. PV contributes only $\approx 0.3\,\text{kA}$ due to inverter current-limiting.	Certain pickup; selective tripping of the faulted ring feeder.
51N (Ground Overcurrent)	Residual current $3I_0$	SLG dominated by zero-sequence contribution from grounded synchronous generators; PV contributes negligible $3I_0$.	Reliable SLG pickup; unaffected by PV presence.
67 (Directional Phase OC)	Direction of positive-sequence current I_1	Clear forward direction toward the faulted section in both PV–ON and PV–OFF conditions.	Correct directional isolation of the faulted feeder.
67N (Directional Ground OC)	Direction of $3I_0$	Residual-current direction clearly indicates a downstream SLG fault.	Accurate directional SLG discrimination.
46 (Negative-Sequence)	Negative-sequence current I_2	SLG produces moderate I_2 for less than 80 ms; PV contribution negligible.	No tripping; unbalance below generator and feeder limits.
49 (Thermal Overload)	I^2t heating	Fault cleared within $\leq 80\,\text{ms}$; thermal energy negligible for lines and transformers.	No thermal element operation.
48 (Motor Stall)	Torque–voltage $T \propto V^2$	Not applicable: Cabina 27 ring does not supply large MV induction motors.	Not applicable.
PV Ride-Through (VRT/FRT)	Voltage sag and frequency deviation	LLL: $V \approx 0\,\text{pu}$ for $\approx 80\,\text{ms}$ (within CEI 0-16 VRT curve). SLG: mild sag. Frequency deviation $< 1\,\text{Hz}$.	**PV remains connected; no inverter dropout expected.**

Table 5.8: Generator protection evaluation for Scenario C

Protection	**Relevant Quantity**	**Analytical Observation**	**Expected Response**
87G/87T (Differential)	Internal fault currents	No differential current or generator/transformer zone disturbance observed.	No trip.
51V / 27 (Undervoltage / V–restrained OC)	Terminal voltage V_t	LLL: $V_t \approx 0\,\text{pu}$ for $\approx 80\,\text{ms}$ (below duration needed for UV trip). SLG: mild sag.	No undervoltage or 51V tripping expected.
78 (Out-of-step)	Rotor angle $\delta(t)$	Rotor-angle trajectories remain fully bounded; no slip cycles or divergence.	No out-of-step tripping.
81U/81O (Under/Over-frequency)	Frequency deviation Δf	Slightly larger post-fault excursions with PV ON, but always $< 1\,\text{Hz}$.	No frequency protection operation.
40 (Loss of excitation)	Reactive-power Q behaviour / field indicators	Generators maintained positive reactive power; no LOE signatures.	No loss-of-excitation trip.
24 (Overexcitation)	V/f ratio	Voltage sag decreases flux; no risk of overexcitation or V/Hz violation.	No overexcitation trip.
46 (Negative sequence)	Negative-sequence current I_2	SLG induces moderate I_2 for a very short duration ($< 80\,\text{ms}$).	No unbalance tripping.
49 (Thermal)	Thermal equivalent I^2t	Fault clearing within $\leq 80\,\text{ms}$ results in negligible heating of windings.	No thermal operation.
Feeder isolation	Incomer/feeder breaker status	Ring-network protection isolates feeders; generator incomers remain closed.	Generators stay online.

5.6 Resiliency Assessment and Islanding Considerations

The analysis of the electrical configuration of the *Gruppo Frigo* reveals a critical lack of redundancy at the medium-voltage (MV) level. Although the chiller system provides component-level redundancy through two independent refrigeration units (FRIGO1 and FRIGO2), the upstream power supply architecture does not offer equivalent system-level redundancy. This creates a structural single point of failure (SPOF) which compromises the operational continuity of the entire chilled-water production subsystem.

5.6.1 Identification of the Single Point of Failure

All transformers associated with the chiller system TR-FRIGO1 (1.6 MVA), TR-FRIGO2 (1.6 MVA), and TR-AUX-FRIGO (1.25 MVA)—are radially connected to a single MV busbar denoted as **Q–GRUPPO FRIGO**. This busbar is supplied through a unique 15 kV cable connection from the main plant board QGMT1, protected by the feeder circuit breaker CB106. No alternative supply path or tie connection is present in the unifilar diagrams. Consequently, any of the following events results in complete de-energization of the chiller system:

- A fault on the busbars of Q–GRUPPO FRIGO,
- A fault on the single 15 kV cable section connecting QGMT1 to Q–GRUPPO FRIGO,
- Failure or maloperation of "CB106" GRUPPO FRIGO main breaker,
- Insulation or equipment failure at the bus couplers.

Under such conditions, both FRIGO1 and FRIGO2, as well as the auxiliary transformer TR-AUX-FRIGO, become simultaneously unavailable. This eliminates the entire chilled-water supply capacity for HVAC and technical room conditioning, with direct consequences for airport operation and thermal stability of critical environments.

5.6.2 Protection Selectivity Limitations

Protection selectivity within the chiller system relies on *logical selectivity* which ensures that internal faults in one refrigeration machine (e.g., at TR-FRIGO1) result in tripping

only the corresponding transformer or MCC feeder, without propagating upstream to CB106. However, this logical selectivity is intrinsically limited:

- It cannot maintain service during a busbar fault at Q–GRUPPO FRIGO;
- It cannot prevent system-wide outage caused by a feeder fault upstream of the chiller bus;
- It does not compensate for the absence of an alternative MV supply path.

Thus, despite having two chillers, the system does not exhibit true redundancy unless the upstream MV infrastructure also provides diversity and fault-tolerant paths.

5.6.3 Consequences for system operation

A fault at Q–GRUPPO FRIGO or its supply feeder results in:

- Loss of all 3.0 MW of refrigeration capacity,
- Loss of auxiliary pumps and control equipment,
- Progressive overheating of occupied areas and sensitive technical rooms,
- Degraded environmental control within 15–20 minutes,
- Potential disruption to airport operations.

This represents a significant resiliency gap for a critical-process energy subsystem in a strategic infrastructure such as an international airport.

5.6.4 Proposed Resiliency Enhancements

Several architectural improvements can be adopted to mitigate the identified SPOF:

1. **Dual-feed configuration**: introduce a second independent 15 kV feeder from a different section of QGMT1 or from QGMT2, providing redundancy at the supply level.
2. **Ring or automatic transfer scheme**: implement a normally-open tie between Q–GRUPPO FRIGO and a neighbouring MV bus to enable automatic re-routing of supply.

3. **Split-bus arrangement**: divide Q–GRUPPO FRIGO into two half-buses, each supplying one refrigeration unit; a bus fault then affects only one machine rather than both.

4. **Bus-tie with directional logic**: install a bus-tie breaker with bidirectional protection to allow temporary bypass during fault clearing.

5. **Independent auxiliary supply**: provide TR-AUX-FRIGO with a redundant feed to ensure compressor auxiliaries remain operational even during bus faults.

These measures significantly enhance the fault tolerance of the chilled-water production system and reduce the risk of simultaneous loss of cooling capacity during MV electrical disturbances. The proposed architectural enhancements are schematically illustrated in Figure 5.15, highlighting the transition from a purely radial configuration to a more resilient supply arrangement.

(a) Current radial configuration (SPOF)

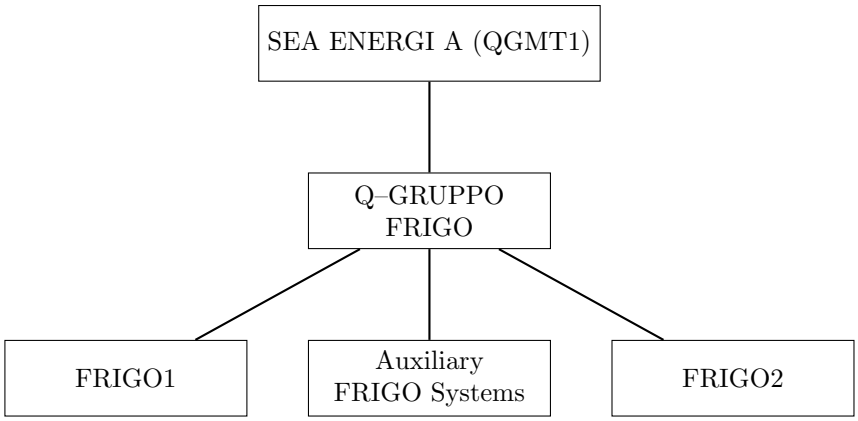

(b) Proposed resilient configuration

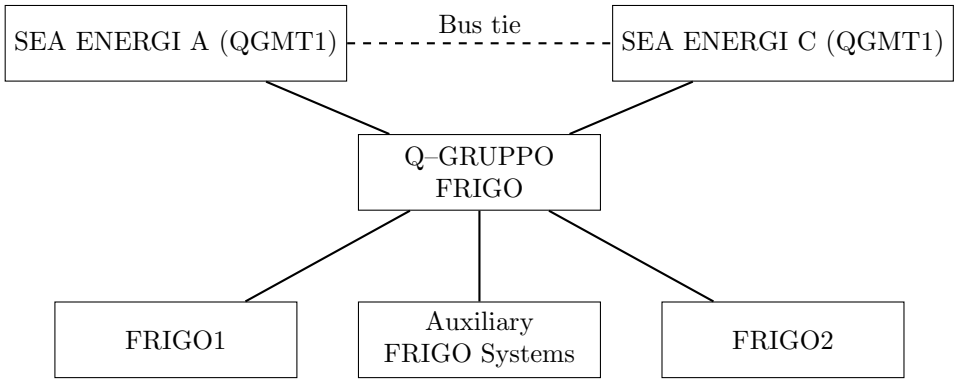

Figure 5.15: Conceptual illustration of resiliency enhancements for the Gruppo Frigo supply: (a) current radial configuration exhibiting a single point of failure at the Q–GRUPPO FRIGO bus; (b) proposed configuration with dual feeding, bus-tie interconnection, and dedicated auxiliary supply, enabling improved fault tolerance and operational resiliency.

5.6.5 Topological Limitation: Inability of the MV Network to Form a Single Coherent Electrical Island

In addition to the Single Point of Failure associated with the radial supply of the *Gruppo Frigo*, a second major resiliency constraint emerges from the structure of the medium-voltage (MV) network itself. Although the Milano Malpensa Airport energy system is operationally capable of functioning in *servizio separato*, as documented in Section 1.9, the present MV topology does not inherently support the formation of a *single coherent electrical island* in the event of loss of supply from the external 132 kV grid. The limitation arises not from the capabilities of the synchronous cogenerators which can independently regulate voltage and frequency during island mode but from the connectivity of the MV network, which tends to fragment into multiple electrically disjoint subsystems immediately after external disconnection.

Under grid-connected conditions, the external transmission system acts as a strong voltage and frequency reference that maintains synchronism across all MV sections of the airport. When the S/S AT point of common coupling (PCC) opens due to an external fault, this external reference is lost, and the electrical coherency of the system becomes entirely dependent on internal topology. In the present configuration, however, the SDC is divided into several MV subsystems—including CENTRALE (QGMT1), SEA ENERGIA A (QGMT2), SEA ENERGIA B (QGMT2),SEA ENERGIA C (QGMT2), the *Gruppo Frigo* supply branch, Cabina 27, and other feeders—that are connected through radial paths or normally open ring sections. Not all these interconnections are designed to be closed or reconfigured automatically during islanded operation, and therefore cannot maintain electrical continuity throughout the SDC.

Once the PCC is opened, the network would consequently separate into multiple uncoordinated electrical islands, each lacking the capability to balance power flows or share stabilising reserves with the others. Since synchronous generators can regulate frequency and voltage only if the system remains electrically unified, the fragmentation of the MV network prevents the airport grid from behaving as a single coherent island. Any attempt by the generators to stabilise multiple isolated segments simultaneously would result in incoherent frequency regulation, uncontrolled voltage divergence, or mancata isola, depending on the specific load-generation imbalance of each segment.

Furthermore, coherent islanding requires real-time automatic coordination, including:

- Rapid closure of MV bus ties to bind the MV network into a single electrical region,

- Synchronised reconfiguration of feeders to maintain load balancing,
- Coordinated allocation of generation between the on-site units,
- Island-mode protection setting groups and dedicated synchronisation logic, and
- Centralised control capable of dispatching active and reactive power across the entire SDC.

None of these functions are presently enabled in the MV network configuration used for modelling in this thesis.

Therefore, while Malpensa Airport can technically operate in island mode under its operational procedures, the current MV topology does not guarantee the formation of a single unified island after external grid loss. Instead, without active network reconfiguration or automatically closed MV bus ties, the system would fragment into multiple independent electrical islands. This constitutes a significant resiliency limitation and highlights the need for structural reinforcement and advanced control strategies if reliable, system-wide island operation is to be ensured.

The topological limitation of the MV network, leading to fragmentation into multiple uncoordinated electrical islands after loss of the external grid, is schematically illustrated in Figure 5.16, Without automated MV reconfiguration or normally closed bus ties, the on-site generation cannot impose a common voltage and frequency reference across all segments, preventing the formation of a single coherent island.

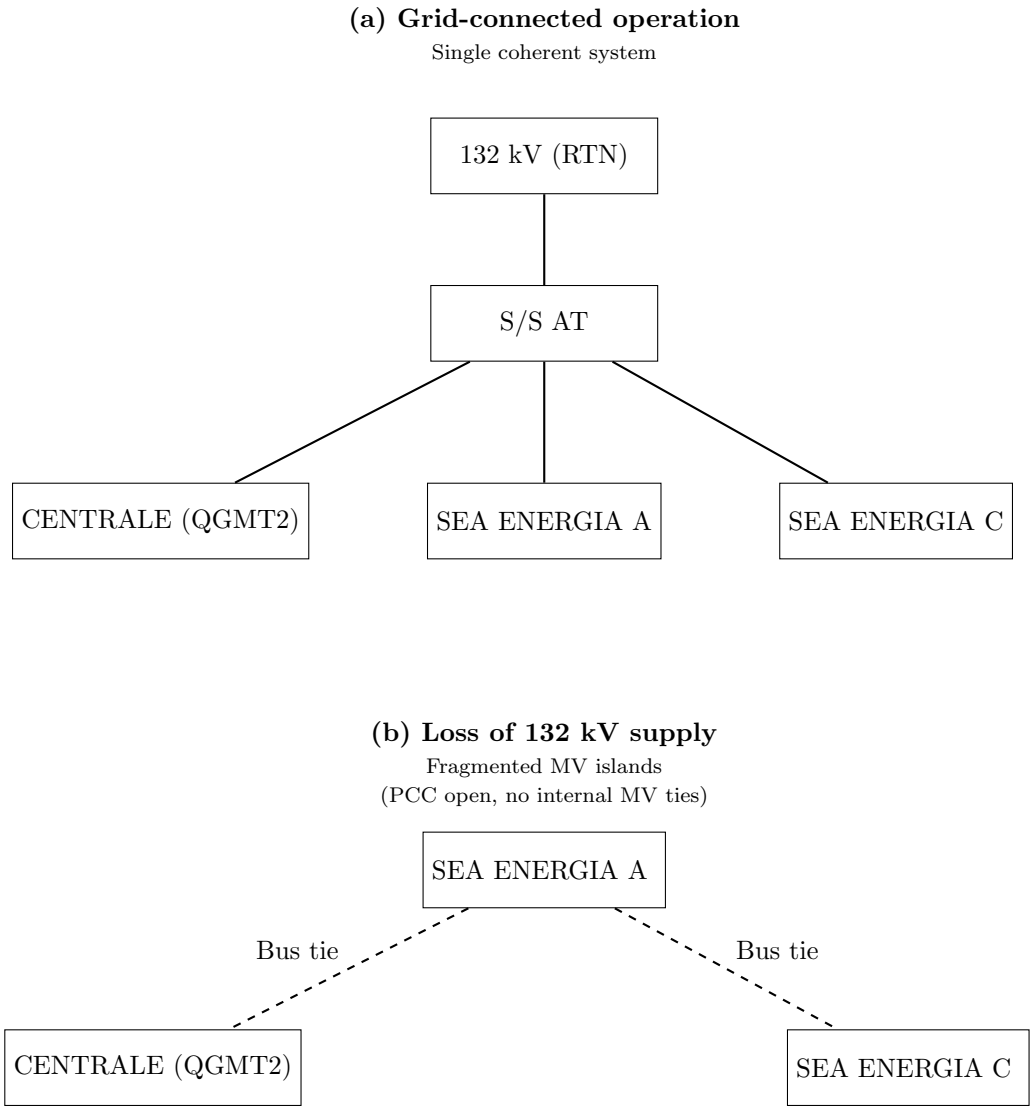

Figure 5.16: Conceptual representation of MV network topology: (a) grid-connected operation, where the external 132 kV system provides a common voltage and frequency reference ensuring coherency across MV subsystems; (b) loss of the external grid, resulting in fragmentation of the MV network into multiple electrically isolated islands due to the absence of internal bus interconnections.

5.6.6 Feasibility of Islanded Operation

Although islanded operation is therefore an *actual capability* of the Malpensa electrical system, a complete transient-stability simulation of the islanding process could not be performed in this study. The limitation does not arise from the absence of islanding functionality in the real system, but from the lack of access to a number of critical modelling parameters required to reproduce island-mode dynamics realistically. These include:

- Generator control configurations and setpoints active exclusively in island mode (e.g. governor droop characteristics, AVR operating modes, frequency-reference logic),
- The detailed islanding-transfer logic implemented at the 132 kV interface,
- Priority-based load-shedding schemes and demand-management policies applied during post-separation transients,
- Dedicated protection setting groups used only during islanded operation,
- Quantitative information on reactive-power dispatch, tap-changing behaviour, and voltage-restoration procedures active in separated operation.

In addition to these unavailable system-specific parameters, a full dynamic study of islanding would require several enabling technologies whose detailed configurations were not provided for modelling purposes. In general, realistic island-mode simulations necessitate:

- Grid-forming sources (such as battery energy storage systems or advanced grid-forming PV inverters),
- Fast and adaptive load-shedding mechanisms to maintain frequency stability,
- a dedicated set of island-mode protection settings and time-coordination curves,
- ROCOF or vector-shift relays for accurate islanding detection,
- MV bus-tie configurations permitting the formation of a single coherent island,
- A centralised energy management system coordinating generation and load.

While some of these capabilities may exist operationally within the Malpensa control architecture, the necessary quantitative data and detailed protection/control logic were

not available for integration into the ETAP transient-stability model. Conducting an islanding simulation without these parameters would result in a model-driven artefact rather than a physically credible representation of the airport's behaviour.

For these reasons, the present analysis focuses exclusively on grid-connected conditions, for which complete data were available and modelling accuracy could be guaranteed. Islanded operation is therefore recognised as an important operational feature of the real system, but is identified as a topic for future research requiring full access to generator, protection, and energy-management configurations specific to servizio separato.

Chapter 6

Summary

This thesis has presented a comprehensive and technically rigorous assessment of the electrical system of Milano Malpensa Airport, combining transient-stability simulations, short-circuit protection analysis, and a structural evaluation of network resiliency. The work was grounded in a detailed modelling framework that included realistic representation of the 132 kV transmission corridor, analytical evaluation of relay behaviour, and the use of systematic event sequencing to reproduce protection-clearing actions within ETAP's Transient Stability module. Together, these modelling strategies ensured that the results obtained were physically credible and consistent with established engineering practice.

A key contribution of the thesis is the verification of *generator stability* under a range of representative disturbances. In Scenario A, severe faults on the 132 kV Turbigo (Linea SEA) interconnection were shown to impose the strongest electromechanical stresses on the system, yet the on-site synchronous generators (TG–E and TV5) maintained stable rotor-angle trajectories and acceptable frequency deviations under both three-phase and single-line-to-ground faults. The clearing time of 60 ms, motivated by the HV protection-coordination framework used by SEA and Terna, proved to be well within the system's stability limits. These results confirm that external transmission-level events, although potentially severe, do not threaten the dynamic integrity of the airport power system.

Scenario B shifted the focus to internal MV disturbances, specifically within the *Gruppo Frigo* subsystem. The simulations confirmed that generator stability is not endangered by internal 15 kV faults, regardless of location or fault type. However, the study identified a significant *architectural vulnerability*: the entire refrigeration infrastructure is radially supplied from a single MV bus (Q–GRUPPO FRIGO), making it

a clear Single Point of Failure. While feeder-level protection correctly isolates only the faulted compressor, a bus-level fault results in a complete loss of refrigeration load. Analytical evaluation of motor protections (49, 46, 48) demonstrated that, for the voltage depressions encountered, no stalling or thermal overload conditions would arise for the large compressor motors. Thus, the primary limitation in Scenario B is *resiliency*, not electromechanical stability.

Scenario C examined disturbances in the looped 15 kV ring beneath Cabina 27, offering a clear contrast to the radial characteristics of Scenario B. The results showed that the ring topology provides greater robustness to contingencies, with directional protection elements correctly discriminating between upstream and downstream faults. The presence of a 10 MW PV plant was found to improve voltage resilience during fault-induced voltage depressions, accelerating post-fault recovery without adversely affecting generator synchronism. As expected for grid-following inverters, the PV plant did not contribute rotational inertia, resulting in slightly larger initial frequency peaks. Nonetheless, all disturbances were successfully ridden through.

A further central contribution of this thesis is the *analytical protection evaluation* performed using IEC 60909 short-circuit currents in combination with time-domain simulated waveforms. This analysis verified the sensitivity, directionality, and selectivity of the principal protection functions (50/51, 51N, 67/67N). Phase and ground-fault currents exceeded protection pickup thresholds by large margins, and fault-direction analysis confirmed that PV integration did not impair directional discrimination. Although ETAP cannot execute relay logic dynamically, the analytical procedure developed in this thesis proved effective and yielded results consistent with expected protection performance.

The resiliency assessment revealed two main structural constraints within the airport distribution system. The most prominent is the Single Point of Failure in the *Gruppo Frigo* supply path, which constitutes a critical operational vulnerability. A second limitation concerns the modelling of islanded operation. As documented in Section 3.9, the Malpensa SDC is technically capable of operating in *servizio separato*, maintaining autonomous frequency and voltage control following separation from the national grid. However, the absence of detailed control parameters, load- shedding sequences, and island-mode protection settings prevented credible simulation of this operational state within the present study. Consequently, islanding could not be included in the transient-stability scenarios, even though it remains an important feature of real-world operation.

Overall, this thesis demonstrates that the Malpensa Airport electrical system is dynamically robust, protection-coordinated, and capable of riding through a wide range of credible disturbances under grid-connected conditions. The main opportunities for improvement lie not in generator stability but in *network architecture and operational coordination*, most notably through the reinforcement of MV redundancy and the development of detailed models to support future island-mode simulations.

The methodological approach developed in this thesis integrating transient stability, analytical protection assessment, and system-resiliency analysis offers a coherent and scientifically rigorous framework that can be extended to future studies or applied to other critical infrastructure electrical networks.

Table 6.1: Summary of transient stability performance

Scenario Description	**Fault Type**	**Minimum Voltage and Frequency**	**Power-Angle Behaviour**	**Fault-On Duration**	**Post-Fault Dynamic Settling Time**	**Stability Outcome**
Scenario A – HV interface at S/S AT (132 kV)	Three-phase (LLL) fault	$V \approx 0$ pu for ∼60 ms; frequency within 49.6–50.4 Hz	Large initial rotor-angle excursion, followed by damped oscillations	∼60 ms	∼10–12 s (decaying electromechanical oscillations)	Stable
Scenario A – HV interface at S/S AT (132 kV)	Single-line-to-ground (SLG) fault	$V \approx 0.7$–0.9 pu; frequency within 49.8–50.2 Hz	Mild rotor-angle oscillations, rapidly attenuated	∼60 ms	∼5–8 s	Stable
Scenario B – MV radial subsystem (Gruppo Frigo, 15 kV)	Three-phase (LLL) fault at Q–GRUPPO FRIGO	$V \approx 0.8$–0.9 pu at generator buses; $\lvert\Delta f\rvert < 0.2$ Hz	Negligible rotor-angle disturbance	∼80 ms	∼2–4 s	Stable
Scenario B – MV radial subsystem (Gruppo Frigo, 15 kV)	Single-line-to-ground (SLG) fault	$V \approx 0.85$–0.95 pu; $\lvert\Delta f\rvert < 0.2$ Hz	No loss of synchronism observed	∼80 ms	∼2–3 s	Stable
Scenario C – MV ring network under Cabina 27 (15 kV, PV ON)	Three-phase (LLL) fault	$V \approx 0$ pu for ∼80 ms; $\lvert\Delta f\rvert < 1$ Hz	Bounded rotor-angle oscillations with additional voltage support from PV	∼80 ms	∼8–10 s	Stable
Scenario C – MV ring network under Cabina 27 (15 kV, PV OFF)	Three-phase (LLL) fault	$V \approx 0$ pu for ∼80 ms; $\lvert\Delta f\rvert < 1$ Hz	Bounded rotor-angle oscillations without PV support	∼80 ms	∼7–9 s	Stable
Scenario C – MV ring network under Cabina 27 (15 kV)	Single-line-to-ground (SLG) fault	$V \approx 0.8$–0.9 pu; $\lvert\Delta f\rvert < 0.5$ Hz	Negligible dynamic impact on generator angles	∼80 ms	∼3–5 s	Stable

Bibliography

[1] T. Kyriakidis *et al.*, "Techno-economic design of energy systems for airport electrification: A hydrogen-solar-storage integrated microgrid solution," *Applied Energy*, 2021.

[2] Jeya Gopi,Arwinder Singh *et al.*, "Mitigation of Voltage Sags by Dynamic Voltage Restorer," *Journal of Automation and Control Engineering*, vol. 2, no. 1, pp. 49–53, 2014.

[3] M. H. J. Bollen, "Understanding power quality problems: Voltage sags and interruptions," ser. Power Engineering, Piscataway, NJ: IEEE Press 2000.

[4] M. Rossi *et al.*, "Resilience in an Evolving Electrical Grid," *Energies*, vol. 14, no. 3, p. 694, 2021.

[5] Terna S.p.A., "Codice di trasmissione, dispacciamento, sviluppo e sicurezza della rete," *Terna – Codice di Rete Italiano*, 2026. Online: https://www.terna.it/it/sistema-elettrico/codici-rete/codice-rete-italiano

[6] Y. Mohamed, "Protection coordination planning with distributed generation," Final Report, CANMET Energy Technology Centre – Varennes, Natural Resources Canada, Rep. CETC-Varennes 2007-149 (TR), June 2007.

[7] Kyriakidis, T., Lanz, G., Cherkaoui, R., & Kayal, M. (2014). *A transient stability assessment method using post-fault trajectories*. EPFL Middle East.

[8] Usman, J., Mustafa, M. W., & Aliyu, G. (2013). Coordination of PSS and FACTS devices for power system stability enhancement: A review of the state-of-the-art. *ARPN Journal of Engineering and Applied Sciences, 8*(5), 369–379.

[9] Huang, J., Rimorov, D., Kamwa, I., Darvishi, A., Fardanesh, B., & Babaei, S. (2020). Advanced controls to improve dynamic stability performance for large power systems. In *IEEE PES General Meeting* (pp. 1–5).

[10] Khamies, M., Magdy, G., Hussein, M. E., Banakhr, F. A., & Kamel, S. (2020). An efficient control strategy for enhancing frequency stability of multi-area power system considering high wind energy penetration. *IEEE Access, 8*, 135144–135159.

[11] Suchithra, K. S., Gopalakrishnan, E. A., Kurths, J., & Surovyatkina, E. (2022). Emergency rate-driven control for rotor angle instability in power systems. *Chaos, 32*(6), 061102.

[12] Abazari, S., Heidari, M., & Abjadi, N. R. (2014). Adaptive control design for a synchronous generator. *Revue Roumaine des Sciences Techniques*, 59(4), 411–421.

[13] Nallagalva, S. K., Kirar, M. K., & Agnihotri, G. (2012). Transient stability analysis of the IEEE 9-bus electric power system. *IJSET, 1*(3), 161–166.

[14] Kotamarty, S. (2006). *Impact of distributed generation on distribution contingency analysis* (Master's thesis). Mississippi State University.

[15] Ochoa, L. F., Da Silva, L. G. W., Harrison, G. P., Padilha-Feltrin, A., & Mantovani, J. R. S. (2005). Index for the evaluation of distributed generation impacts on distribution system protection. In *UPEC 2005* (pp. 1–5).

[16] Tariq, A., Khatri, K. L., Haque, M. I. ul, Raza, M. A., Ahmed, S., & Muzammil, M. Investigation of the effects of distributed generation on protection coordination of a power system. *NED University of Engineering and Technology & Sir Syed University of Engineering and Technology.*

[17] Sharafutdinov, K., Rydin Gorjão, L., Matthiae, M., Faulwasser, T., & Witthaut, D. (2018). Rotor-angle versus voltage instability in the third-order model for synchronous generators. *arXiv:1706.06396.*

[18] El Idrissi, Z., El Mariami, F., Belfqih, A., & Haidi, T. (2021). Impact of distributed power generation on protection coordination in distribution networks. *Indonesian Journal of Electrical Engineering and Computer Science, 23*(3), 1271–1280.

[19] Agbetuyi, A. F., Bango, O., Abdulkareem, A., Awelewa, A., Somefun, T., & Olubunmi, A. (2021). Investigation of the impact of distributed generation on power system protection. *ASTESJ, 6*(2), 324–331.

[20] Eltamaly, A. M., Mohamed, Y. S., El-Sayed, A. H., & Elghaffar, A. N. (2019). Reliability/security of distribution system network under supporting by distributed generation. *Insight - Energy Science, 2*(1), 1–14.

[21] Takele, H. (2022). Distributed generation adverse impact on the distribution networks protection and its mitigation. *Heliyon, 8*, e09624.

[22] Iliev, I., Kryukov, A., Bulatov, Y., Suslov, K., Beloev, I., & Valeeva, Y. (2025). Methods for ensuring stability of operating conditions of an electric power system with distributed generation plants. *IJPEDS, 16*(1), 138–150.

[23] Thapa, J., & Maharjan, S. (2019). Impact of penetration of photovoltaic on rotor angle stability of power system. *IJEAS, 6*(4), 112–117.

[24] Genc, I., & Usta, O. (2005). Impacts of distributed generators on the oscillatory stability of interconnected power systems. *Turkish Journal of Electrical Engineering & Computer Sciences, 13*(1), 149–161.

[25] Barsoum, N., Zulkeffley, N., & Songkin, M. (2018). Transient stability simulation of 33 kV power grid. *Energy and Power Engineering, 10*(6), 301–318.

[26] IEEE Power Engineering Society. (2002). *IEEE Std 1110-2002: IEEE guide for synchronous generator modeling practices and applications in power system stability analyses*. IEEE. (Reaffirmed 2019).

[27] Grainger, J. J., & Stevenson, W. D., Jr. (1994). Chapter 12: Unsymmetrical faults. *Power System Analysis*, McGraw–Hill, pp. 470–523.

[28] Glover, J. D., Overbye, T. J., & Sarma, M. S. (2017). *Power system analysis and design* (6th ed.). Cengage Learning.

[29] Kundur, P. (1994). *Power system stability and control*. McGraw–Hill.